



Review

Photocatalytic mineralization of hydrogen sulfide as a dual-phase technique for hydrogen production and environmental remediation

Kumar Vikrant^a, Ki-Hyun Kim^{a,b,*}, Akash Deep^{c,***}^a Department of Civil and Environmental Engineering, Hanyang University, 222 Wangsimni-Ro, Seoul 04763, Republic of Korea^b Henan Province Engineering Research Center for Forest Biomass Value-added Products, Henan Agricultural University, Zhengzhou 450002, China^c Central Scientific Instruments Organization (CSIR-CSIO), Sector 30 C, Chandigarh 160030, India

ARTICLE INFO

Keywords:
 Photocatalysis
 Odor
 H_2S
 Pollution control
 Hydrogen production

ABSTRACT

Hydrogen sulfide (H_2S) is regarded as a broad-spectrum poison associated with severe health consequences. Among the available treatment options, photocatalytic technology may be effectively applied to the production of hydrogen gas through the splitting of H_2S molecules and the addition of 79.9 kJ mol^{-1} of energy. As a result, advanced photo-reactive media may provide a win-win strategy to treat the parent pollutant (H_2S) while producing hydrogen gas. This review encompasses both TiO_2 and non- TiO_2 catalysts capable of operating under ultraviolet, visible, and solar light irradiation. The performances of photocatalysts are assessed in terms of quantum yield, space-time yield, and other operational variables, including mode of operation, irradiation time, and relative humidity. The concept of space velocity is used to compare photocatalysts in reference to benchmark parameters for the treatment of H_2S . This review addresses current limitations and future prospects of the application of photocatalytic technology to efficiently mitigate H_2S pollution.

1. Introduction

The development of mitigation strategies for numerous hazardous compounds [1,2] has been the subject of considerable research effort in response to growing concerns over the scope of environmental pollution and associated health effects. Hydrogen sulfide (H_2S) is a highly toxic and malodorous pollutant (with its characteristic rotten-egg odor) [3–5]. As a broad-spectrum toxin, H_2S can damage multiple parts of the body, including the central nervous system, at concentrations higher than 100 ppm [6,7]. The toxicity of H_2S originates with its tendency to combine with iron-bearing mitochondrial cytochrome enzymes, resulting at elevated concentrations (e.g., at ≥ 200 ppm) in insensibility or death due to asphyxiation [6,8]. In addition, brief exposure to H_2S at ≥ 50 ppm or extended exposure at 5–10 ppm may lead to olfactory fatigue (deadening of the sense of smell) and cause a person to lose the ability to detect many toxic substances, even at deadly concentrations [9,10].

A number of techniques have been developed over the years to treat H_2S -laden air: (i) nondestructive approaches such as adsorption [11–14], scrubbing [15,16], and membrane filtration [17,18]; (ii) destructive approaches including photocatalysis [19–22], biodegradation [6,23,24], and thermal/catalytic oxidation [25,26]. Among the

abovementioned techniques, the use of organic amine solutions (e.g., ethanamine) was made preferably in various industries as they are an effective option to scrub acidic compounds (e.g., H_2S) from gaseous effluents [27,28]. However, as scrubbing systems suffer from a number of shortcomings (e.g., difficult handling, low regenerability, slippage, thermal degradation, and temperature swing parasitic energy losses), they are often an unfavorable option in economical sense [29,30]. In addition to scrubbing, the use of adsorption-based approaches is found commonly in several industries to efficiently control the emission of hazardous gaseous pollutants owing to their economical and flexible nature [31–33]. Likewise, the potential utility of conventional adsorbents like activated carbon and inorganic materials (such as silica and alumina) has been investigated for the removal of H_2S . However, their applications were often restricted due to low performance as they lack target-specific functionalities to treat lower molecular weight pollutants such as H_2S [32,33]. Consequently, caustic impregnated activated carbons were often utilized in practice due to their enhanced removal capacity of gaseous odorants (e.g., H_2S) [34,35]. However, such caustic impregnated adsorbents employ catalytic mechanisms to remove H_2S which leads to the deposition of elemental sulfur on the sorbent surface [36,37]. As such sulfur deposits render the sorbents non-regenerable for further cycles, their application is often confined to

* Corresponding author at: Department of Civil and Environmental Engineering, Hanyang University, 222 Wangsimni-Ro, Seoul 04763, Republic of Korea.

** Corresponding author.

E-mail addresses: kkim61@hanyang.ac.kr (K.-H. Kim), a.deep.phd@gmail.com (A. Deep).

only one-time usage [34,37]. In addition to the severe drawback (e.g., in terms of non-reusability), such chemically enhanced adsorbents are very expensive to restrict their usage [34]. Notably, the membrane-based approaches have also attracted a wide attention in recent years owing to their distinctive merits (e.g., easy operation, less space requirement, and low maintenance cost) [38,39]. However, the membranes are not suitable enough for applications under harsh real-world conditions as they can be subject to reduced selectivity under low flux conditions and/or reduced permeability over long term usage (e.g., due to the adsorption of multicomponent pollutants onto the polymeric membrane matrix) [33,38–40]. Also, the bio filtration-based system was once proposed as a cost effective and ecofriendly option to treat gaseous pollutants [6,24]. However, as the bio filtration of H₂S produces sulfuric acid, it can severely inhibit the microbial growth to restrict the transfer of H₂S into the biofilm (at low pH condition) [6,41,42]. Note that some specific microbial strains were identified to be capable of tolerating highly acidic conditions (acidophilic bacteria). Nonetheless, the performance of such biofilter setups has usually been estimated to be insufficient for recommendation in a real-world industrial setting [24,43,44]. Also, such biological processes are highly dynamic in nature to require regulation of various variables (e.g., temperature, pH, and biofilm nutrient level) to maintain the optimal conditions for the microbial activities. As such, such option is also unsuitable for practical purposes [6,24].

The modified Claus process, a destructive thermocatalytic technique that recovers elemental sulfur from gaseous H₂S, is one of the most widely used industrial techniques to treat H₂S-laden streams [45–47]. It is nonetheless found that such process has a demerit of producing tailgases rich in hazardous pollutants (e.g., SO_x, CS₂, and COS). As those components are often hydrolyzed to yield H₂S itself, further retreatment step is demanded to resolve such problems [45,48]. Additionally, the decomposition of H₂S into elemental sulfur through the Claus process (~60% conversion efficiency) requires significantly high temperatures (~1500°C) [49]. In order to enhance its conversion efficiency (to reach up to 99.9%), precious metal-based catalysts (e.g., Pt) are often employed at the expense of drastically increased operational costs [45,49]. Also, additional specific equipment is often required to avoid the formation of hazardous fog during the condensation of produced sulfur vapors in the Claus process [45]. In this regard, despite the fact that the Claus process is a mature technology being implemented worldwide for the recovery of sulfur from H₂S rich industrial effluents, there is a widespread research interest to develop new and less convoluted H₂S management strategies with high performance to overcome its limitations (e.g., with respect to the requirement of high temperature combustion furnace, waste heat boiler system, condensers, multi-bed catalytic conversion systems, customized sulfur condensing systems, and tail-gas management systems) [45,50,51]. Moreover, the energy stored in H₂S is practically wasted by the Claus process, as it is preferentially consumed to produce water instead of hydrogen as a motive for the new research interests towards alternative technologies [50,52].

Among a myriad of alternatives, the photocatalytic approach offers many advantages. It generates environmentally benign end products, operates under ambient conditions, and can degrade a wide range of hazardous pollutants [53–55]. For H₂S treatment, photocatalytic technology has been employed to split H₂S molecules into hydrogen gas [19]. Low-cost methods of hydrogen production are highly sought after, as hydrogen is a clean energy carrier [56]. Photocatalytic splitting of water is among the most promising of hydrogen-production options [57,58] but photocatalytic treatment of toxic H₂S molecules to produce hydrogen gas requires significantly less energy compared with techniques that split water (79.9 kJ mol⁻¹ vs. 285.8 kJ mol⁻¹) [19,59].

This review highlights recent developments in photocatalytic treatment of H₂S, and includes an in-depth analysis of the performance of photocatalysts in terms of their quantum yield (QY) and space-time yield (SY). A brief attempt is made to compare the performances of photocatalytic and adsorption systems based on the concept of space

velocity. In addition, prevailing reaction pathways coupled with corresponding by-products are identified and reported. The limitations of photocatalytic technology are also evaluated. This article offers intriguing insights into the application of photocatalysts toward intelligent mitigation options for H₂S pollution and associated areas of investigation.

2. Gaseous photocatalytic systems

Research and development of photocatalysts that can remediate gaseous pollution (e.g., volatile organic compounds and odorants) is growing rapidly due to the technology's multiple advantages and practical efficiency [60–62]. Because photocatalysts often yield environmentally benign end products, no subsequent or additional stages are needed to manage the disposal of by-products [61]. In contrast, adsorption technology requires ancillary steps (e.g., frequent regeneration or multiple repetitive runs) [63]. Additionally, during regeneration, adsorbed pollutants may inadvertently be liberated back into the atmosphere, and additional steps to manage by-product disposal can be required. A photocatalytic approach may offer a superior solution if an appreciable level of efficiency can be achieved under real-world conditions [64,65].

A photocatalyst is a semiconducting material that exploits the energy of irradiated light (of suitable wavelength) to degrade and mineralize compounds into less toxic or low-impact end products [53,54]. The most important step in a photocatalytic process is the formation of electron-hole pairs (e⁻-h⁺) through: (i) illumination of catalyst particles by a suitable light source, (ii) absorption of photons with sufficient energy, and (iii) transition/promotion of electrons from the valence to conduction band (Fig. 1) [53,66]. Holes generated in the valence band and electrons in the conduction band thermodynamically reduce oxygen or water molecules to yield highly reactive radicals (e.g., O₂^{·-} and OH[·]) (Fig. 1) [54]. Prominent examples of semiconducting photocatalysts used in industrial processes include TiO₂-based catalysts, metal sulfide-based catalysts (e.g., CdS and ZnS), and other metal oxide-based catalysts (e.g., WO₃, MoS₂, and Fe₂O₃) [61,67,68].

In gas-phase reactions, the overall transfer of pollutant molecules from the bulk to external surface of the photocatalyst can greatly influence reaction rates or net photocatalytic efficiency [66]. Thereafter, the molecules of the target pollutant adsorb and diffuse into the porous network of the photocatalyst and eventually react with radical species to yield compounds that are lighter than raw targets (Fig. 1) [69,70]. Essentially, a large amount of the produced e⁻-h⁺ pairs recombine either after reaching the catalyst surface or during their journey to the surface (volume recombination) [71,72] (Fig. 1). Their recombination leads to the dissipation of the harvested light energy in the form of light emission (radiative loss) or heat (nonradiative loss) [72,73]. The annihilation of e⁻-h⁺ pairs result in the lowering of net quantum yield and overall photocatalytic performance [71,74]. Thus, a practical photocatalytic material should be able to favorably extend the lifespan of photo generated e⁻-h⁺ pairs so that they can effectively survive long enough to participate in redox reactions with the adsorbed target species [67,75]. The fundamental mechanisms involved in photocatalysis have been discussed in detail elsewhere [2,54,55,72,76,77]. Also, its reaction pathways, as illustrated in Fig. 1, have been discussed in detail in Section 4. The performances of photocatalysts used for the abatement of gaseous H₂S are summarized in Table 1 and discussed in subsequent subsections. All catalysts are classified as either TiO₂-based or non-TiO₂-based.

2.1. TiO₂-based catalysts

The vast majority of the published literature indicates that TiO₂-based catalysts have been the prime focus of photocatalytic research owing to their abundance, low cost, chemical stability, and non-toxicity [61,78,79]. However, practical use of TiO₂ for the treatment of gaseous

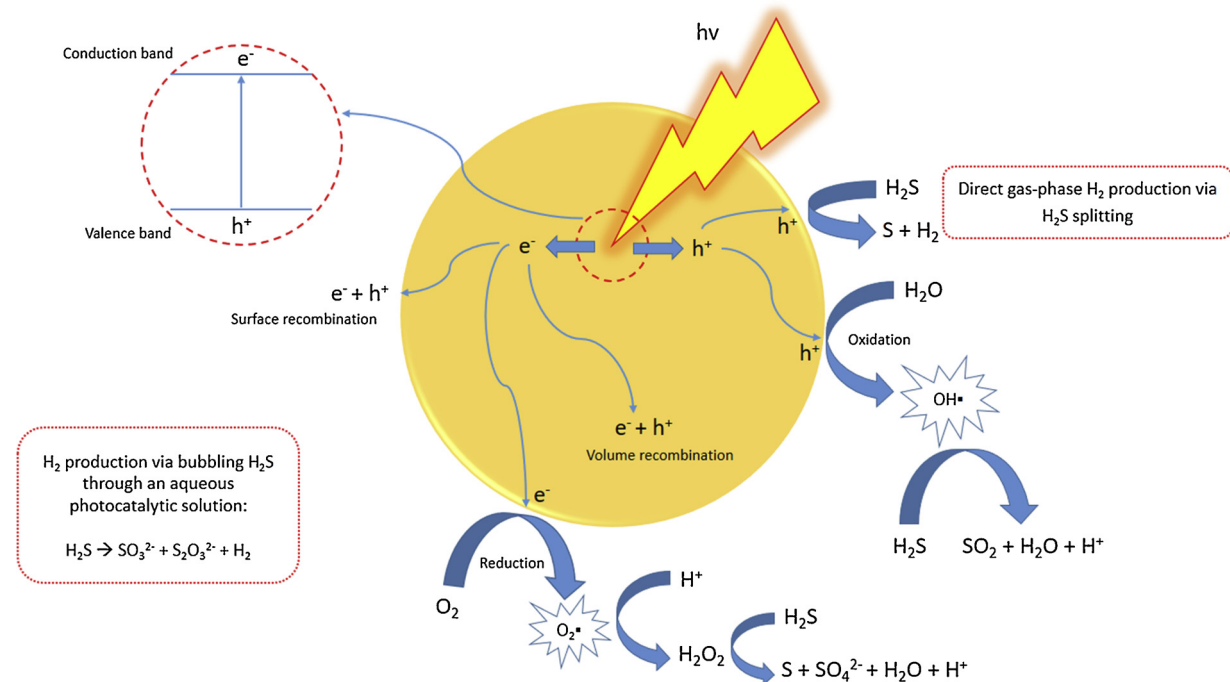


Fig. 1. Schematic of the fundamental mechanisms and reactions involved in the photocatalytic removal of gaseous H₂S as well as production of hydrogen (from the splitting of H₂S molecule).

pollutants under real-world conditions faces several hurdles, including frequent deactivation and unsatisfactory performance [65,69,80]. Deactivation of pristine TiO₂ can be ascribed to the blockage of surface active sites by sulfate or sulfur deposits formed by the oxidation of H₂S [81]. Also, the formation of toxic, malodorous, and corrosive sulfur dioxide (SO₂) species during photocatalysis has restricted the practical application of TiO₂ [82]. The use of support materials has been proposed as an effective strategy to overcome these limitations and boost photocatalytic performance [83,84]. An ideal supporting material should have a high surface area, be porous, inexpensive, and stable under irradiated light, and exhibit large affinity for the target pollutant [85,86]. As can be seen from Table 1 and subsequent discussions, zeolite, SiMgO_x, glass, ceramics, nickel foam, and fibrous materials have been utilized as effective support materials for the photocatalytic removal of gaseous H₂S.

Zeolite has been suggested as a promising support material as it can effectively separate photo-generated charge carriers (e⁻-h⁺ pairs) to prolong their recombination and effectively adsorb the produced SO₂ to avoid its liberation [87,88]. A TiO₂/zeolite photocatalyst demonstrated outstanding performance in the oxidation of H₂S in a simulated biogas environment (QY of 1.01E-04 molecules photon⁻¹ and SY of 5.02E-07 molecules photon⁻¹ mg⁻¹) [87] (Table 1). Biogas is a sustainable and renewable energy source that can replace natural gas in industries and domestic households [6,89]. However, first it needs to be upgraded to eliminate toxic components (e.g., H₂S) to avoid health risks, corrosion of storage tanks and pipelines, and the generation of hazardous by-products upon combustion [89,90]. As biogas contains large quantities of carbon dioxide (CO₂), the physicochemical properties of which resemble that of H₂S, it is imperative for the photocatalyst to have positive selectivity toward H₂S to avoid any competitive effects [13,91].

The selectivity and performance of TiO₂/zeolite composite toward the oxidation of H₂S in a biogas mimic has been ascribed to the intensification of H⁺ abstraction in the Lewis basic sites of TiO₂ [87,92]. Also, the presence of CO₂ (under moist conditions) did not affect the photocatalytic oxidation of H₂S by TiO₂ or TiO₂/zeolite (due to high H₂S selectivity and photocatalytic enhancement by moisture). Nonetheless, the presence of CO₂ caused significantly adverse effect on H₂S

adsorption as zeolite's sorption sites became saturated with CO₂ molecules (Fig. 2) [87]. Another porous material, SiMgO_x (with a high specific surface and porosity) has also been suggested as a base support for TiO₂ due to its adsorptive tendency and low cost [92]. Additionally, SiMgO_x may aid in the migration of highly reactive free radicals [93]. A TiO₂-SiMgO_x composite demonstrated a promising performance in the destruction of H₂S (QY of 1.41E-05 molecules photon⁻¹ and SY of 9.42E-08 molecules photon⁻¹ mg⁻¹) [93] (Table 1).

To delay the recombination of photo-generated e⁻-h⁺ pairs, the formation of heterojunctions through a combination of TiO₂ and other semiconducting materials has been called a suitable route [94,95]. The use of TiO₂ ultraviolet (UV) 100 has been recommended over TiO₂ P25 due to the former's higher surface area, which should facilitate elevated adsorption of H₂S onto O-Ti⁴⁺ sites, along with a higher generation of OH[·] [81,96]. Moreover, TiO₂ UV 100 may lower or delay the liberation of SO₂ coupled with heightened storage of sulfates so that the deactivation of the photocatalyst is delayed [81]. In this regard, a WO₃/TiO₂ UV 100 heterojunction performed well in the photocatalytic destruction of H₂S (QY of 8.38E-05 molecules photon⁻¹ and SY of 1.99E-07 molecules photon⁻¹ mg⁻¹) [81] (Table 1).

The efficiency of photocatalytic technology can also be enhanced with thin films that are attached strongly to a substrate material such as ceramics or glass [97,98]. Paints are being considered as a suitable option for mixing photocatalysts as they can be effectively applied to existing surfaces [99,100]. The use of paints to mix photocatalysts particles may also reduce consumption of the catalyst compared with their use in powdered form [101]. A TiO₂-based acrylic paint performed well in the photocatalytic destruction of H₂S (QY of 1.30E-05 molecules photon⁻¹ and SY of 2.77E-09 molecules photon⁻¹ mg⁻¹) [102] (Table 1). The Langmuir-Hinshelwood kinetic model has been described as the best fit for the observed data, as mass transfer did not play a major role in governing photo-degradation kinetics [102]. TiO₂-coated glass fibers also performed well in the photocatalytic destruction of H₂S (QY of 8.60E-05 molecules photon⁻¹ and SY of 2.15E-08 molecules photon⁻¹ mg⁻¹) [103] (Table 1).

In recent years, demands have been growing to utilize vacuum UV (VUV) irradiation for the effective removal of gaseous odors

Table 1
Gas-phase photocatalytic systems for the treatment of H_2S .

Order	Photocatalyst	Light source	Reactor	Mass of catalyst (mg)	Concentration (ppm)	Irradiation time (h)	Relative humidity (%)	Conversion (%)	Quantum yield (molecules photon $^{-1}$ mg^{-1})	Space-time yield (molecules photon $^{-1}$ mg^{-1})	Space velocity (h $^{-1}$)	Reference
[A] TiO_2-based catalysts												
1	Mn-TiO_2	Two 4 W VUV lamps	Continuous-flow fixed-bed glass tube (500 mL)	1000	150	1	50	89.9	3.76E-03	3.75E-06	1.12E-02	[112]
2	TiO_2 P25 coating	Two 8 W and 15 W UV backlight tubes	Single-pass annular Pyrex reactor (166 mL)	600	100	6	NA	80	7.77E-04	1.29E-06	1.11E-02	[134]
3	$\text{TiO}_2/\text{zeolite}$	One 40 W UV lamp with a 365 nm wavelength	Fixed-bed made of glass tube (21 mL)	200	Simulated biogas containing 1000 ppm H_2S	5	NA	90	1.01E-04	5.02E-07	7.51E-03	[87]
4	WO_3/TiO_2 UV 100 photocatalyst	One 8 W backlights UV tube with 365 nm wavelength	Single-pass annular Pyrex reactor (100 mL)	420	15	20	NA	100	8.38E-05	1.99E-07	5.96E-04	[81]
5	$\text{TiO}_2\text{-SiMgO}_x$	Two 8 W UVA	Plug flow reactor with a Pyrex glass window	150	15	12	30	90	1.41E-05	9.42E-08	5.63E-04	[93]
6	Ti-Cr-MCM-48	One 8 W backlights UV tube with 365 nm wavelength	Glass tubular catalytic bed (0.6 mL)	40	35	7.9	NA	92	3.55E-06	8.87E-08	3.31E-03	[123]
7	TiO_2 -coated glass fiber filter	One 100 W visible filament lamp	Annular tubular borosilicate glass reactor (1017 mL)	4,000	14	1	65	99	8.60E-05	2.15E-08	1.20E-04	[103]
8	TiO_2 -based acrylic paint	Four 250 W UV mercury vapor lamps	Continuous-flow rectangular reactor	4,700	31	2.5	NA	94	1.30E-05	2.77E-09	1.03E-03	[102]
9	$\text{TiO}_2/\text{zeolite}$	One 40 W UV black light tube with a 365 nm wavelength	Single-pass cylinder column (12.7 mL)	NA	Simulated biogas containing 1000 ppm H_2S	5	NA	98.1	1.10E-04	NA	NA	[214]
10	$\text{TiO}_2\text{-SiMgO}_x$	Two 8 W VUV lamps	Continuous-flow flat reactor with a top borosilicate glass	NA	15	12	30	80	1.26E-05	NA	NA	[92]
11	TiO_2 coating	Microwave electrodeless discharge lamps (165 W)	Microwave photocatalytic reactor	NA	3.6	1	NA	61	5.94E-06	NA	NA	[115]
12	TiO_2 coated foam nickel support	Three 8 W UV lamps	Synthetic glass tubular reactor (120,000 mL)	NA	144	3	80	97	NA	NA	NA	[131]
13	TiO_2 on a fibrous support	Three circular lamps emitting UV-A (90 W/m 2) and VIS (60 W/m 2)	10 mm quartz tube	400	2,000	6.5	NA	80	NA	NA	NA	[138]
[B] Non-TiO_2 catalysts												
1	$\text{CdS-ZnS/Fe}_2\text{O}_3$	Visible-light lamp (34 W) with 400–800 nm wavelength	Packed bed reactor made of borosilicate tube (350 mL)	1000	25	1	NA	92	7.56E-06	7.55E-09	9.59E-05	[144]
2	CdS/CdWO_4	One visible-light Xe lamp (350 W)	Cylindrical quartz thermostatic reactor	500	NA	3	NA	NA	NA	NA	NA	[152]
3	FeMM	One 100 W UV mercury lamp	Quartz reactor (12 mL)	NA	NA	0.5	NA	99.1	NA	NA	NA	[153]

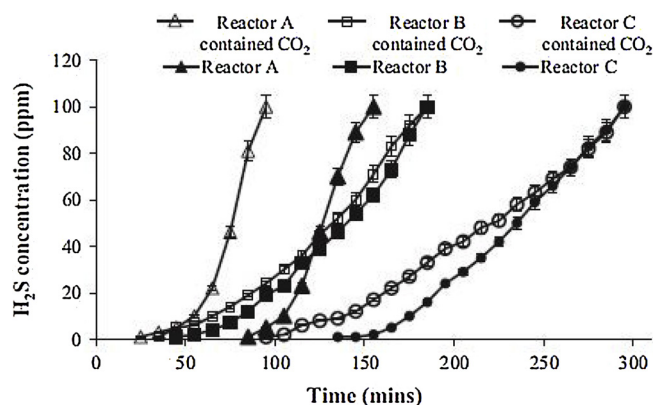
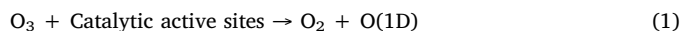


Fig. 2. Effect of CO_2 on H_2S removal in reactors A, B, and C containing zeolite, TiO_2 , and TiO_2 /zeolite, respectively; reproduced with permission from [87].

[104,105]. Approximately 8% of VUV consists of ~ 8% of 185 nm wavelength energy with the remaining irradiation measuring 254 nm [106]. VUV irradiation consists of high-energy photons that activate water and oxygen molecules to yield highly reactive species such as O_3 , OH^\cdot , $\text{O}(3\text{P})$, and $\text{O}(1\text{D})$ [107]. Despite its advantages, VUV irradiation alone may not yield sufficient O_3 gas [108,109]. The formation of O_3 is needed to initiate *in situ* decomposition of H_2S molecules via direct photo oxidation or catalytic ozonation [110,111]. However, the use of VUV irradiation to degrade target pollutant molecules may be vindicated in combination with other techniques such as photocatalysis [107,110]. In this regard, the use of Mn- TiO_2 demonstrated outstanding performance in degrading H_2S molecules under VUV irradiation (QY of 3.76E-03 molecules photon $^{-1}$ and SY of 3.75E-06 molecules photon $^{-1}$ mg $^{-1}$) [112] (Table 1). The active sites present in Mn- TiO_2 decompose residual O_3 molecules to produce $\text{O}(1\text{D})$ and OH^\cdot species to enhance H_2S degradation (Eqs. 1 and 2).



The considerable reduction rate of O_3 at the reactor outlet suggests Mn- TiO_2 under VUV irradiation is an effective remediation option [112]. In another report made for the effective utilization of a powerful and potent light source, the use of a microwave electrodeless discharge lamp (MEDL) was recommended to enhance the photocatalytic destruction of target pollutants. An MEDL can generate UV-vis radiation through the absorption of microwave power while simultaneously producing highly reactive oxygen species (OH^\cdot , O_2^\cdot , and O_2^\cdot) [113–115]. A TiO_2 coating effectively improved the photocatalytic performance of a 165 W MEDL in H_2S destruction (QY of 5.94E-06 molecules photon $^{-1}$) [115] (Table 1). Interestingly, a potent role for reactive oxygen species in the degradation of H_2S was evident as there was no photocatalytic degradation of H_2S in a purely nitrogen atmosphere [115].

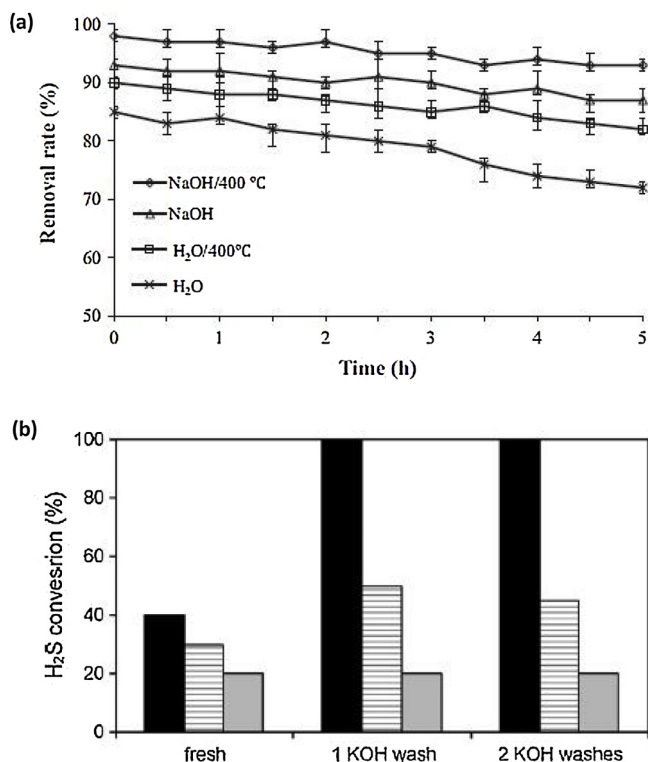
Based on the above discussions and reported literature, a strategy to enhance the rate of reaction and/or overall removal efficiency should be based on increasing the intensity of incident light on the photocatalyst surface or using a potent light source with shorter wavelength [116,117]. Notably, for the same distribution of photonic energy, i.e., the same prominent wavelength, an increase in the incident light intensity can favorably help increase the quantities of e^- - h^+ pairs (as the number of photons hitting the catalyst surface increases manifold) [118,119]. Interestingly, under a high pollutant concentration and low intensity of the irradiated light, a first-order kinetics is often observed to overshadow e^- - h^+ recombination with the prevailing redox reactions [80,118]. In contrast, for low pollutant loading and high intensity light, a half-order kinetics is often observed. Such an occurrence is ascribed to the predominant recombination of e^- - h^+ pairs as the number

of adsorbed pollutant molecules is relatively low to take part in redox reactions [80]. In addition, the usage of highly powerful light sources may cause unnecessary hike in capital and operational costs. Also, the use of VUV or MEDL should be made with caution although they may be useful in enhancing the overall removal efficiency. However, one should be cautious on their adverse effects, as a large portion of the produced O_3 and other active oxygen species may escape the reactor (if the residence time is low) [80,112,115].

One of the major drawbacks of pristine TiO_2 is that it can function only under UV irradiation, which is less than 4% of the solar spectrum [120]. To overcome this limitation, incorporation of transition metal ions into TiO_2 has been recommended for the expansion of overall operating conditions (e.g., under visible-light irradiation) [121,122]. For instance, Ti and Cr species were immobilized in the pores of mesoporous silica, MCM-48, which has a three-dimensional, continuous and interwoven porous structure, is an efficient support for TiO_2 . The resulting Ti-Cr-MCM-48 photocatalytic system was operated under visible light to degrade H_2S (QY of 3.55E-06 molecules photon $^{-1}$ and SY of 8.87E-08 molecules photon $^{-1}$ mg $^{-1}$) [123] (Table 1). The enhanced performance of Ti-Cr-MCM-48 under visible light was ascribed to the ligand-to-metal charge transfer excitation of highly dispersed Cr^{6+} ions, which facilitated the transfer of electrons from O^{2-} to Cr^{6+} ($[\text{Cr}^{6+}\text{-O}^{2-}] [\text{Cr}^{5+}\text{-O}]^*$) [124]. As an electron was donated by the Cr^{5+} species to nearby Ti-O moieties, it was scavenged by O^\cdot species to enhance the separation of charges [124]. Ti-Cr-MCM-48 did not produce toxic SO_2 gas during H_2S oxidation (due to high selectivity for specific catalytic reactions) but it suffered from severe deactivation (due to sulfate deposition and conversion of Cr^{6+} to Cr^{3+}) [123,125].

In order to expand the applicabilities of pristine TiO_2 into the visible-light domain, intrinsic self-doping of oxygen vacancies in the parent TiO_2 structure has been investigated as an effective route (in addition to the common option like the incorporation of transition metal ions) [126,127]. Particularly, bridging oxygen vacancy (BOV) defects in the rutile TiO_2 (110) structure can be introduced through vacuum annealing or hydrogen reduction approach. The BOV defects, if occurring, can act as active centers for H_2S adsorption to enhance its conversion efficiencies. Additionally, the presence of such defects can also assist favorably in prolonging the lifespan of e^- - h^+ pairs to avoid or suspend their recombination for the noticeable upgrades in photocatalytic performance [126,128,129]. Further, the BOV sites can also act as electron donors that can effectively dissociate the adsorbed H_2S molecules. Note that an energy barrier of only 1.4 eV (much larger for defect-free TiO_2 surfaces) needs to be overcome by the BOV sites to dissociate H_2S molecules into HS/H and $\text{S}/\text{H}/\text{H}$ [130]. According to the density functional theory (DFT) calculations, the optimal BOV site should be located at the bridged O_{2c} atom to support the existence of an isolated defect level within the band gap structure of the photocatalyst [130].

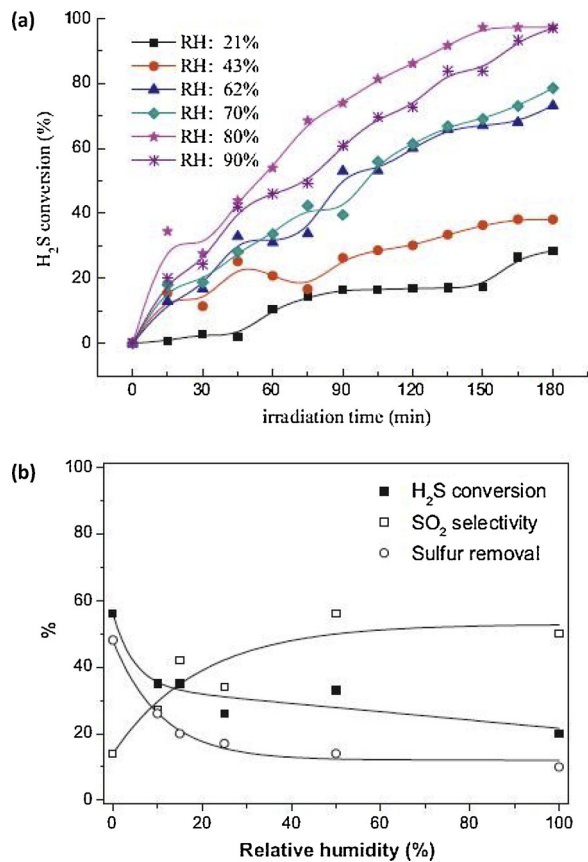
The effective regeneration of spent photocatalysts is of prime importance from a practical viewpoint. Catalyst deactivation may be both reversible (if it is governed by weak adsorption of partially oxidized products or other compounds) or irreversible (if it is involved strong deposition of non-volatile products such as sulfate) in nature [92]. In the case of reversible deactivation, a catalyst may simply be treated by UV irradiation, temperature rise, or a current of fresh air [92,131]. However, for irreversible deactivation, a specific chemical treatment may be required to regenerate a photocatalyst [87,92]. Calcination and washing with a weak base have been recognized as effective methods to regenerate spent TiO_2 /zeolite composites after their use for oxidation of H_2S from biogas [87] (Fig. 3a). In fact, washing with distilled water only led to partial regeneration of the catalyst (Fig. 3a). Calcination enhanced the dispersion of TiO_2 on zeolite, which reduced the effect of active-site blockage by sulfate/sulfur deposition [132,133]. Further, treatment with a weak base efficiently altered the surface isoelectric point of TiO_2 /zeolite to yield a negatively charged surface that can favorably adsorb acidic H_2S molecules while removing sulfate [134].



Similarly, washing a spent TiO₂-SiMgO_x composite with 1 M KOH solution resulted in an enhanced adsorption of H₂S molecules, as it caused the removal of deposited sulfurous compounds while providing new basic sites on the catalyst surface [92] (Fig. 3b). In addition, treating the spent TiO₂ P25 coating with 0.01 M NaOH solution induced full recovery of photocatalytic activity [134]. In another experiment, an effective regeneration of a deactivated, TiO₂-coated, foam nickel support was undertaken by irradiating the spent photocatalyst sample with an O₃ lamp (185 nm) for two days [131].

Relative humidity has also been found to influence photocatalytic removal of H₂S. The presence of moisture can inhibit adsorption of H₂S molecules [135,136]. At times, water and H₂S molecules compete for available sorption sites (surface-OH sites for water molecules), while Ti⁴⁺ sites compete for H₂S molecules. Consequently, the presence of water may lead to partial or complete formation of layers on the catalyst surface that restrict the access of the H₂S molecules to the Ti⁴⁺ sites [134]. In some cases, the presence of moisture can boost photocatalytic oxidation due to the formation of OH[·] radicals from the interaction of water molecules with photo-generated holes [80,137].

The presence of moisture was reported to make a mixed contribution to the photocatalytic performance of TiO₂/zeolite toward H₂S [87]. The control experiments in the presence of moisture saw a decrease in H₂S adsorption by zeolite but enhanced photocatalytic oxidation by TiO₂. The presence of moisture in a biogas mimic was found to retard the production of SO₂/SO₃ during H₂S oxidation by TiO₂/zeolite, as the produced SO₂/SO₃ was converted into SO₃²⁻/SO₄²⁻ through interactions with water molecules [87]. Interestingly, TiO₂-coated foam nickel support was associated with a sharp rise in H₂S conversion efficiency as the relative humidity level rose from 21 to 80% (Fig. 4a) [131]. Overall H₂S conversion was reduced beyond 80% possibly due to the competitive adsorption process between water and H₂S molecules (Fig. 4a)



[131]. In another study, an increase in the photocatalytic conversion efficiency of TiO₂-SiMgO_x for H₂S was observed up to a relative humidity of 30% (T = 30 °C). The performance eventually declined upon further increase in moisture content [92].

In contrast, a TiO₂ P25 coating is reportedly the best H₂S conversion option in the absence of moisture (QY of 7.77E-04 molecules photon⁻¹ and SY of 1.29E-06 molecules photon⁻¹ mg⁻¹) (Fig. 4b) [134]. The reduced photocatalytic performance of the TiO₂ P25 coating in the presence of moisture was ascribed to the restricted access to sorption sites for H₂S molecules due to the formation of water layers on the surface (through which the H₂S molecules must diffuse to reach the active catalyst surface) [134]. A similar observation was also reported when TiO₂ was used with a fibrous support. The presence of moisture reduced H₂S conversion primarily due to the inhibitory effects of the formed water layers on the photocatalyst surface [138]. On many occasions, the literature is contradictory with respect to the effect of relative humidity on the efficiency of H₂S photocatalysis. This contradictory role of moisture content regarding the performance of photocatalysts can arise due to various effects as described above. Photocatalytic performance can be improved through the formation of OH[·], although it can also be suppressed by other factors (e.g., competitive adsorption between H₂S and water molecules on the catalyst surface). Consequently, the full aspects of such effects need to be evaluated to properly optimize a given photocatalytic system.

2.2. Non-TiO₂-based catalysts (metal sulfides and oxides)

Owing to the restrictive capabilities of TiO₂ (e.g., low quantum efficiency, swift deactivation, and ability to work only under UV irradiation), substantial efforts have been made to develop alternatives [139,140]. However, with respect to the photocatalytic removal of H₂S, little attention has been paid to the development of non-TiO₂ catalysts, unlike the other targets (e.g., volatile organic compounds) [141,142].

Due to its narrow band gap (2.4 eV), CdS has been being widely investigated as a catalyst for visible-light-driven photocatalytic applications [139]. CdS-based catalysts have exhibited excellent photocatalytic behavior owing to their superior capacity for mobilizing photo-generated e⁻-h⁺ pairs with delayed recombination [143]. A CdS-ZnS/Fe₂O₃ photocatalyst was effectively applied to the decomposition of gaseous H₂S under 34 W of visible light irradiation (400–800 nm wavelength) (QY of 7.56E-06 molecules photon⁻¹ and SY of 7.55E-09 molecules photon⁻¹ mg⁻¹) [144] (Table 1). Relatively rapid deactivation of the catalyst surface was observed at higher flow rates due to sulfate/sulfur deposition. The observations indicated that the kinetics of H₂S mass transfer from the bulk to the photocatalyst surface play major roles in the effective oxidation of H₂S molecules [144].

The coupling of two semiconductors through the synthesis of composite materials is an effective approach to improving photocatalytic performance. Apart from favoring superior absorption, photocatalytic efficiency can be amplified in the visible-light region along with other beneficial factors, such as an improved range of operating redox potential and better control of charge recombination [145–147]. Metal tungstates can enhance the favorable physicochemical characteristics of photocatalytic systems due to self-trapped excitations and a layered structural framework [148–150]. Among various tungstates, CdWO₄ has been recognized as an attractive option; its monoclinic-layered wolframite framework provides highly favorable chemical, optical, and structural characteristics coupled with high thermal stability [150,151]. CdWO₄ nanorods sensitized with CdS nanoparticles (CdS/CdWO₄) yielded a composite material with good performance in photocatalytic removal of H₂S under visible light irradiation (350 W Xe lamp) [152] (Table 1). Due to a lack of reported data (e.g., applied concentration, removal percentage), the QY and SY values could not be derived for certain case studies (Table 1). Both CdS-ZnS/Fe₂O₃ and CdS/CdWO₄ were developed primarily for hydrogen production via H₂S splitting in the gas phase; their applications are discussed in detail in Section 3 [144,152]. Natural Tagan montmorillonite in its iron form (FeMM) also performed well in removing H₂S from petroleum industry effluent, achieving a 30 min conversion rate of 99.1% under UV irradiation. The same conversion percentage was achieved after 7 min under solar irradiation [153] (Table 1). An increase in the amount of divalent iron in the FeMM structure (11% to 22%, along with a simultaneous decrement in the amount of paramagnetic trivalent iron species) was observed after H₂S treatment, indicating a major involvement of trivalent iron in controlling the photocatalytic efficiency of FeMM [153].

3. H₂S splitting and hydrogen production

As a potentially clean energy carrier, hydrogen has been the target of considerable research efforts across the globe [154,155]. It has the highest energy density (120–142 MJ kg⁻¹) of all fuels without a carbon trace [156]. As such, the demand for novel strategies capable of producing hydrogen economically are high. The production of hydrogen via water splitting with the aid of a TiO₂ photocatalyst was first demonstrated in 1972 [157]. The years since have witnessed a rapid rise in efforts to produce hydrogen from water using diverse photocatalysts under solar light irradiation based on its practical merits (e.g., economical, clean, and low-impact operation) [56,58]. The photo-splitting of H₂S requires less than a third of the energy required for water splitting (79.9 kJ mol⁻¹ for H₂S compared with 285.83 kJ mol⁻¹ for

water) [59]. The production of hydrogen and sulfur via photo-splitting of H₂S may provide a potential win-win strategy as there is a pressing need from an environmental perspective to safely dispose of H₂S [20,156]. The produced hydrogen can be used as a clean energy carrier while the generated sulfur may find its way to agricultural, pharmaceutical, and associated industries [59].

In the quest to develop suitable photocatalysts for H₂S splitting, metal sulfides have emerged as suitable candidates owing to their ability to resist deactivation while maintaining stability in sulfur-rich media [158–160]. Additionally, the use of metal sulfides for photocatalytic splitting of H₂S may help address a serious drawback common to photocatalysts, i.e., rapid corrosion by photo-generated holes. In metal sulfides, the photo-generated holes effectively react with H₂S molecules to yield sulfur (Eq. 3) leaving no holes to cause undesired photo-corrosion reactions [158].



The practical applicability of single-phase metal sulfides photocatalysts has been restricted due to their poor ability to absorb solar light and the rapid recombination of photo-generated charge carriers [161,162]. To resolve such limitations, synergistic combinations of heterojunctions and solid solutions have been devised to guarantee enhanced visible-light absorption capabilities coupled with effective sulfur desorption capacity while avoiding rapid deactivation [158,163]. To this end, MnS (with a band gap of 3.7 eV) was synergistically combined with In₂S₃ (band gap of 2.0–2.3 eV). This composite has been proposed to efficiently produce hydrogen via H₂S splitting (maximum hydrogen evolution rate of 8360 μmol h⁻¹ g⁻¹) [158] (Table 2). On similar lines, MnS/In₂S₃-MoS₂ displayed an excellent maximum hydrogen evolution rate of 49,600 μmol h⁻¹ g⁻¹ [164] (Table 2). Its enhanced performance was attributed to the formation of a Schottky junction in the heterostructure which efficiently delayed the recombination of photo generated charge carriers [165,166]. The generation of an internal electric field between In₂S₃ and MnS facilitated the separation of photo generated charge carriers. Additionally, the photo generated electrons were preferentially transferred to the MoS₂ structure to promote a further separation of e-h⁺ pairs [164,167]. Interestingly, the combination of both exposed edges in the MoS₂ structure and the presence of unsaturated S atom sites further stimulated the photocatalytic reactions to considerably amplify the overall hydrogen production reactions [164]. In a similar study, PdS was effectively dispersed onto MnS/In₂S₃ and anchored onto In₂S₃ through the formation of Pd-S-In bond so as to achieve an effective separation of photo generated charge carriers [168]. The MnS/In₂S₃/PdS composite photocatalyst showcased a maximum hydrogen evolution rate of 22,700 μmol h⁻¹ g⁻¹ [168] (Table 2). In addition, the presence of PdS was observed to facilitate the desorption of deposited sulfur (end product of H₂S splitting) to help enhance its catalytic performance [168]. Interestingly, the results of an isotope experiment in which H₂S was dissolved in deuterium water (D₂O) yielded the production of D₂ (~10% from D₂O), H₂ (~90% from H₂S), and HD (negligible) during the photocatalytic process [168,169]. The results of this isotope experiment indicated that the hydrogen was evolved due mainly to the photocatalytic H₂S splitting while the contribution from water itself is negligible [169].

Similarly, a MnS/(In_xCu_{1-x})₂S₃ photocatalyst has been demonstrated with exceptional capability to absorb visible light (e.g., up to 599 nm). This system resulted in a hydrogen production rate of 29,252 μmol h⁻¹ g⁻¹ [156] (Table 2) (Fig. 5a). In another work, the incorporation of Cu into crystalline β-In₂S₃ was reported to synthesize an (In_xCu_{1-x})₂S₃ composite, which exhibited enhanced visible-light (300 W Xe lamp with a cutoff filter ($\lambda > 420$ nm)) absorption and efficient desorption of sulfur from the photocatalyst surface after its use [156]. The heightened mobility and separation of photo-generated charge carriers was attributed to the formation of a heterojunction between (In_xCu_{1-x})₂S₃ and γ-

Table 2
Photocatalytic systems for the production of hydrogen via H_2S splitting.

Order	Photocatalyst	Light source	Reactor	Mass of catalyst (mg)	Concentration	Irradiation time (h)	Maximum hydrogen evolution rate ($\mu\text{mol h}^{-1} \text{g}^{-1}$)	Reference
[A] Aqueous systems								
1	$\text{MnS}/(\text{In}_x\text{Cu}_{1-x})_2\text{S}_3$	Visible-light Xe lamp (300 W) with a wavelength $> 420 \text{ nm}$ One solar light Xe lamp (300 W)	Pyrex flask (50 mL) Cylindrical quartz reactor (700 mL)	2.5 500	Bubbling of 3 M H_2S through a solution containing 0.1 M Na_2S and 0.6 M Na_2SO_3 Bubbling of H_2S gas through a 0.5 M KOH solution	6 3	29,252 8880	[156] [59]
2	Bi_2S_3 flowers	One solar light Xe lamp (500 W)	Double-walled cylindrical glass vessel (50 mL)	200	Bubbling of H_2S gas through a 0.5 M NaOH solution to reach a saturated sulfide concentration of 16 g L^{-1}	3	8391	[20]
3	$\text{Fe}_{0.2}(\text{III})\text{Co}_x(\text{III})\text{Zn}_{0.7-x}$	Visible-light Xe lamp (300 W) with a wavelength $> 420 \text{ nm}$ One solar light Xe lamp (300 W)	Pyrex flask (50 mL) Cylindrical quartz reactor (200 mL)	2.5 200	Bubbling of H_2S through a solution containing 0.1 M Na_2S and 0.6 M Na_2SO_3 Bubbling of H_2S gas through a 0.25 M KOH solution	6 7	8360 29,705	[158] [189]
4	$\text{MnS}/\text{In}_2\text{S}_3$	Visible-light Xe lamp (300 W) with a wavelength $> 420 \text{ nm}$ One solar light Xe lamp (300 W)	Double-walled cylindrical glass vessel (50 mL)	200	Bubbling of H_2S gas through a 0.5 M NaOH solution to reach a saturated sulfide concentration of 16 g L^{-1}	3	4,466	[184]
5	$\text{N-TiO}_2/\text{Gr}$	One solar light Xe lamp (500 W)	Cylindrical quartz thermostatic reactor	500	Bubbling of H_2S gas through a 0.1 M KOH solution	3	7812	[152]
6	Ag-doped $\text{Fe}_{0.2}(\text{III})\text{Zn}_{0.7}$	One solar light Xe lamp (500 W)	Double-walled cylindrical glass vessel (50 mL)	200	Bubbling of H_2S gas through a 0.5 M NaOH solution to reach a saturated sulfide concentration of 16 g L^{-1}	3	4,466	[184]
7	CdS/CdWO_4	One visible-light Xe lamp (350 W)	Cylindrical quartz thermostatic reactor	500	Bubbling of H_2S gas through a 0.1 M KOH solution	3	7812	[152]
8	$\text{Cd}_2\text{S}/\text{TiO}_2$ core-shell	One solar light Xe lamp (260 W)	Single port quartz photoreactor	NA	0.3 M ($\text{Na}_2\text{S} + \text{Na}_2\text{SO}_4$)	4	41,600	[174]
9	$\text{MnS}/\text{In}_2\text{S}_3\text{-MoS}_2$	Visible-light Xe lamp (300 W) with a wavelength $> 420 \text{ nm}$	Pyrex flask (50 mL)	2.5	Bubbling of 3 M H_2S through a solution containing 0.1 M Na_2S and 0.6 M Na_2SO_3	3	49,600	[164]
10	$\text{MnS}/\text{In}_2\text{S}_3/\text{PdS}$	Visible-light Xe lamp (300 W) with a wavelength $> 420 \text{ nm}$	Pyrex flask (50 mL)	2.5	Bubbling of H_2S gas through a solution containing 0.1 M Na_2S and 0.6 M Na_2SO_3	5	22,700	[168]
[B] Gaseous systems								

(continued on next page)

Table 2 (continued)

Order	Photocatalyst	Light source	Reactor	Mass of catalyst (mg)	Concentration	Irradiation time (h)	Maximum hydrogen evolution rate ($\mu\text{mol h}^{-1} \text{g}^{-1}$)	Reference
1	$\text{CdS-ZnS/Fe}_2\text{O}_3$	Visible-light lamp (34 W) with 400-800 nm wavelength	Packed bed reactor made of borosilicate tube (350 mL)	2,000	25 ppm	1	6.5E-04	[144]

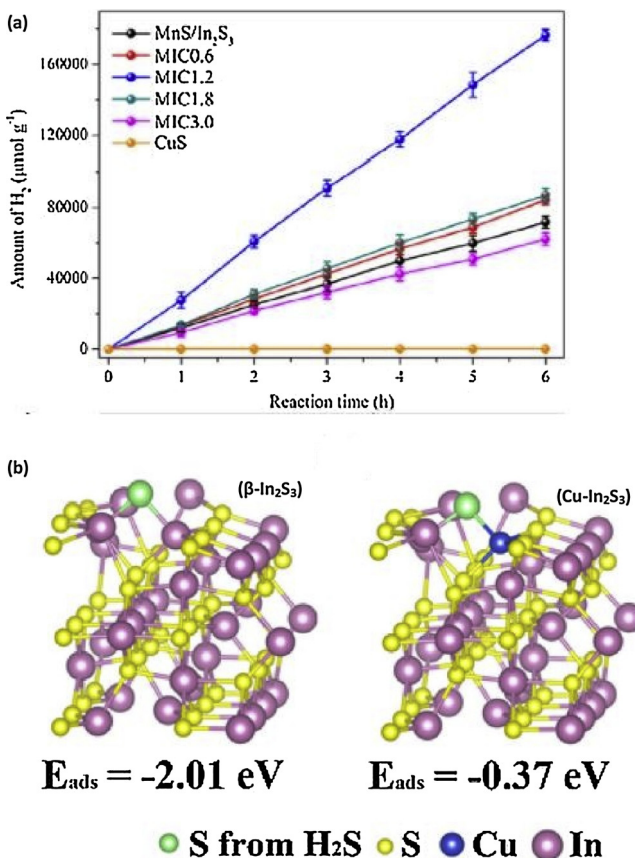


Fig. 5. Photocatalytic splitting of H_2S by $\text{MnS}/(\text{In}_{\text{x}}\text{Cu}_{1-\text{x}})_{2}\text{S}_3$. Panel (a): Hydrogen production by various samples. Note that MIC0.6, MIC1.2, MIC1.8, and MIC3.0 represent the catalysts synthesized using 0.6, 1.2, 1.8, and 3.0 mL of 0.05 M $\text{Cu}(\text{Ac})_2\text{H}_2\text{O}$ /pyridine. Panel (b): The structures of S adsorbed on the surface of β -In₂S₃ and Cu-In₂S₃; reproduced with permission from [156].

MnS [156]. DFT analyses were also presented to show that the presence of Cu promotes desorption of sulfur from a photocatalyst surface. The less negative value of adsorption energy (E_{ads}) for Cu-In₂S₃ (compared with β -In₂S₃) led to prolonged operation without significant deactivation (Fig. 5b).

Another metal sulfide, Cu₂S has attracted great interest in the photocatalytic research toward the harnessing of solar/visible light owing to its significantly narrow band gap (1.8–2.4 eV) [170–172]. However, as pristine Cu₂S particles are often prone to rapid photo corrosion, their direct applications are often found to be unsuitable [171,173]. In this regard, combining Cu₂S with other well-known photocatalysts (e.g., TiO₂) in a core-shell like morphology was proposed as a novel strategy to overcome such drawbacks while boosting the performance under solar light irradiation [174]. Consequently, Cu₂S/TiO₂ core-shell particles were demonstrated to yield an excellent maximum hydrogen evolution rate of 41,600 $\mu\text{mol h}^{-1} \text{g}^{-1}$ under solar light irradiation [174] (Table 2). In case of core-shell-based photocatalytic structures, the shell acted as a co-catalyst for surface reactions whereas the core acted as a photosensitizer [175,176]. Notably, the shell thickness needs to be optimized for such core-shell nanostructures, as it could sensitively affect the performance in many respects. In case of a smaller shell thickness, the recombination of photo generated charge carriers may be prominent, as the core might receive large amounts of incident light [177,178]. On the other hand, if the shell thickness is too large, the light penetration to the core may reduce drastically to lower the photocatalytic performance [177]. Further, the photocatalytic performance of Cu₂S/TiO₂ core-shell particles was observed to decline after the 5th cycle due to the blockage of catalytically

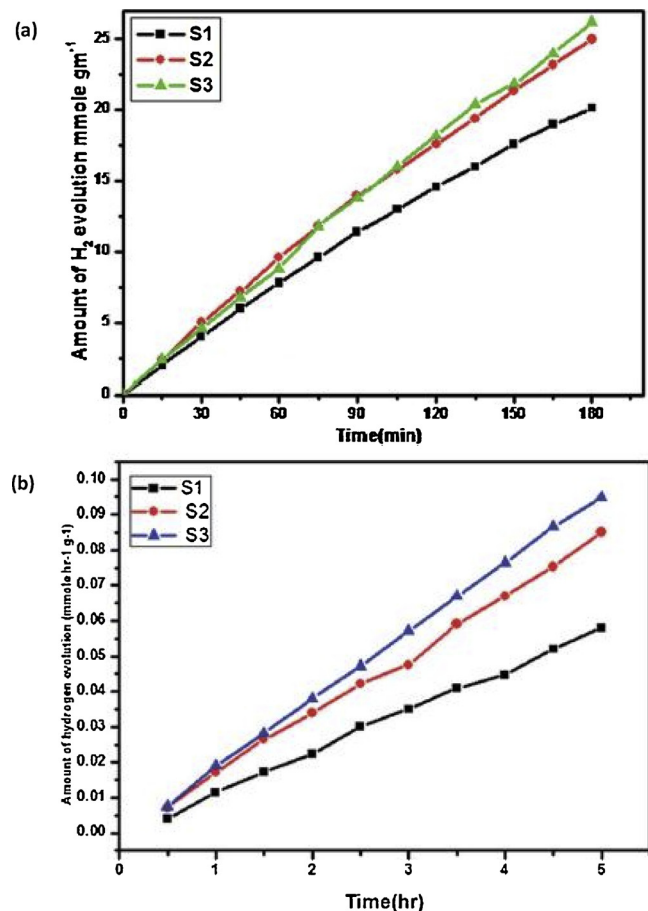


Fig. 6. Utilization of Bi_2S_3 for the production of hydrogen. Panel (a): H_2 splitting. Panel (b): Water splitting. Note that S1 represents Bi_2S_3 particles synthesized using water as a solvent, whereas S2 and S3 represent Bi_2S_3 particles synthesized using a 1:3 mixture of water and ethylene glycol as the solvent with reaction times of 24 and 30 h, respectively; reproduced with permission from [59].

active sites by reaction between intermediates and end-products (not identified in the study) [174].

Among a wide array of reported metal sulfides, Bi_2S_3 has also attracted wide attention as an effective photocatalyst due to a narrow direct band gap (1.3–1.7 eV) [179,180]. For example, Bi_2S_3 particles with flower-like morphology were utilized to efficiently generate hydrogen (e.g., at a rate of 8880 $\mu\text{mol h}^{-1} \text{g}^{-1}$) via H_2S splitting under solar light irradiation [59] (Table 2). A comparison of the efficiency of Bi_2S_3 photocatalyst toward water and H_2S splitting revealed its superior capability for the latter case. The maximum hydrogen evolution rate by Bi_2S_3 was ~467 times larger for H_2S splitting than for water splitting (i.e., 8880 and 19 $\mu\text{mol h}^{-1} \text{g}^{-1}$ for H_2S and water, respectively). This observation was another indicator of the usefulness of photocatalytic splitting of H_2S molecules with respect to both environmental protection and generation of a green fuel (Fig. 6). To boost the photocatalytic activity of metal sulfides, doping of the parent structure with transition metals has been proposed. Such an approach reportedly increases the absorption of photons, improves the separation of photo-generated charge carriers, and enhances the specific surface area of the photocatalyst [181,182]. In particular, the doping of metal sulfides with cobalt could substantially boost photocatalysis of H_2S [13]. In addition, a composite of $\text{Fe}_{0.2}^{(\text{III})}\text{Co}_x^{(\text{III})}\text{Zn}_{0.7-x}^{(\text{II})}\text{S}$ has demonstrated the ability to produce hydrogen via H_2S splitting under solar irradiation (maximum hydrogen evolution rate of 8391 $\mu\text{mol h}^{-1} \text{g}^{-1}$) [20] (Table 2). The entire system yielded higher oxidation states, and the presence of cobalt played an important role in trapping photo-generated holes; the above

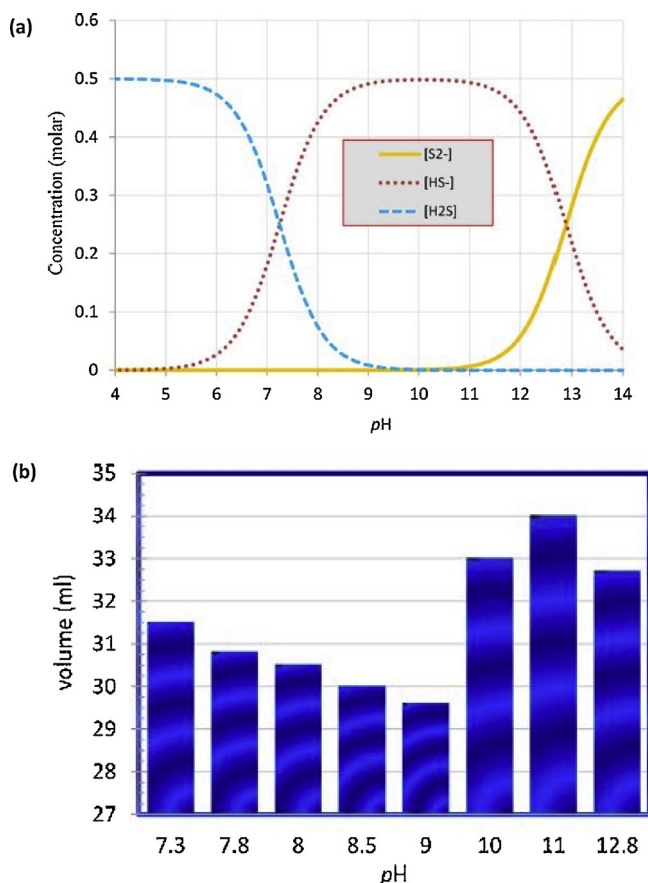
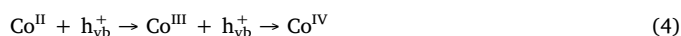
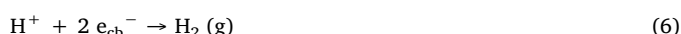


Fig. 7. Utilization of Ag-doped $\text{Fe}_{0.2}^{(\text{III})}\text{Zn}_{0.7}^{(\text{II})}\text{S}$ for the production of hydrogen. Panel (a) Concentration of sulfide (S^{2-}), bisulfide (HS^-), and H_2S species determined theoretically as a function of pH in 0.5 M sodium sulfide aqueous solution. Panel (b): Volume of hydrogen gas evolved from the H_2S solution at different pH values after 90 min of operation for 0.2 g of the photocatalyst; reproduced with permission from [184].

factors combined to cause deacceleration of $\text{e}-\text{h}^+$ recombinations (Eq. 4) [183].



Transient $\text{Co}^{\text{III/IV}}$ species can donate buffered/trapped holes (h_{t}^+) to HS^- ions (the dominant form of H_2S at a pH of 11 in an aqueous solution) at the photocatalyst surface and revert back to the Co^{II} form [184] (Eq. 5) (Fig. 7a). The produced protons subsequently react with photo-generated electrons and catalyze the evolution of hydrogen gas [185] (Eq. 6).



In a similar approach, Ag-doped $\text{Fe}_{0.2}^{(\text{III})}\text{Zn}_{0.7}^{(\text{II})}\text{S}$ demonstrated a high production capacity for hydrogen via H_2S splitting under solar irradiation (maximum hydrogen evolution rate of $4470 \mu\text{mol h}^{-1} \text{g}^{-1}$) [184] (Table 2). As with $\text{Fe}_{0.2}^{(\text{III})}\text{Co}_x^{(\text{II})}\text{Zn}_{0.7-x}^{(\text{II})}\text{S}$, maximum hydrogen production by Ag-doped $\text{Fe}_{0.2}^{(\text{III})}\text{Zn}_{0.7}^{(\text{II})}\text{S}$ was observed at a pH of 11 (Fig. 7b). At pH values > 11 , bisulfide and protons were accompanied in low concentrations, which also caused a decrease in hydrogen evolution. Under acidic conditions, H_2S became the dominant species and readily liberated from the reaction solution, which was responsible for attenuated hydrogen production [20,184]. CdS/CdWO_4 has also been reported with enhanced capacity for hydrogen production via H_2S splitting under visible light (maximum hydrogen evolution rate of $7812 \mu\text{mol h}^{-1} \text{g}^{-1}$) [152] (Table 2).

As mentioned earlier, pristine TiO_2 particles suffer from swift deactivation and low quantum efficiency. Doping of the parent photocatalyst by transition metals often turned out to be an efficient option to upgrade performance. However, in the case of TiO_2 , such a step can exert a negative effect through the acceleration of electron-hole recombination because the metallic centers offer numerous defect sites that can act as recombination centers for photo-generated charge carriers [186,187]. Nonetheless, doping TiO_2 with anions has been suggested as a potential strategy to attain enhanced absorption of visible light [188]. If the p orbitals of anionic dopants overlap with the O2P orbital of TiO_2 the photocatalyst may become suitable with delayed electron-hole recombination [189]. As described earlier, the use of a suitable support material is an effective option to significantly enhance photocatalytic performance. In this regard, graphene has been widely recognized for its thermal conductivity, high surface area, mechanical sturdiness, and ultrahigh charge-carrier mobility [190,191]. When nitrogen-doped TiO_2 was supported onto graphene, the resulting $\text{N-TiO}_2/\text{Gr}$ composite had enhanced potential to produce hydrogen via H_2S splitting under solar irradiation (maximum hydrogen evolution rate of $29,705 \mu\text{mol h}^{-1} \text{g}^{-1}$) [189] (Table 2). The optimum dose of graphene for the photocatalytic composite was 2% [189]. Higher graphene content may block the surface active sites of N-TiO_2 , leading to decreased photocatalytic activity [189].

As can be seen in Table 2, most studies of photocatalytic H_2S splitting for hydrogen production have been conducted in aqueous solutions. Few studies are available on gas-phase H_2S splitting. In one representative study, a $\text{CdS-ZnS}/\text{Fe}_2\text{O}_3$ photocatalyst displayed a maximum hydrogen evolution rate of $6.5\text{E-4} \mu\text{mol h}^{-1} \text{g}^{-1}$. In general, gas-phase systems exhibit relatively poor performance in hydrogen production [144] (Table 2). In a gas-phase system, hydrogen production is generally achieved using systems with relatively low H_2S concentrations (Fig. 8). In continuous-mode gaseous systems, lower H_2S concentrations are likely to slow down adsorption rates and enhance the efficacy of photocatalytic splitting [144].

4. Reaction pathways and product analysis

The end products of a photocatalytic reaction can be predicted and confirmed based on theoretical and practical observations. Photocatalytic reactions may not reach completion under practical situations due to deactivation/inefficiency of the catalyst, presence of competitive effects, and/or excess or lack of moisture [65,192]. Studies that outline the prevalent reaction mechanisms and pathways during the photocatalytic treatment of H_2S are useful to ensuring or enhancing the efficiency of the overall process and amplify its applicability under real-world conditions [65]. The generation of $\text{e}^-\text{-h}^+$ pairs through light

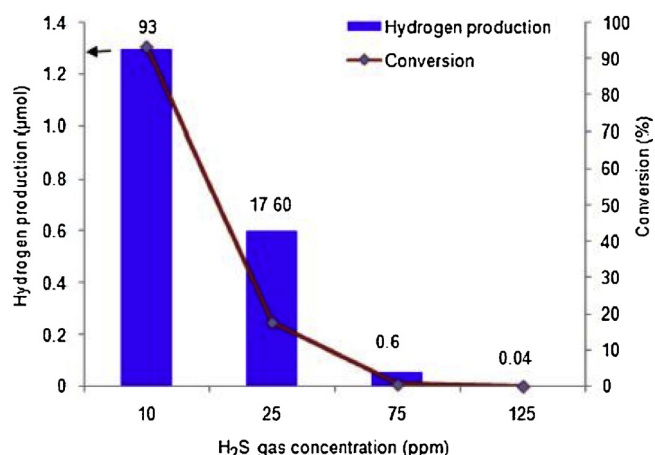


Fig. 8. Effect of H_2S concentration on photocatalytic hydrogen production by $\text{Cds-ZnS}/\text{Fe}_2\text{O}_3$; reproduced with permission from [144].

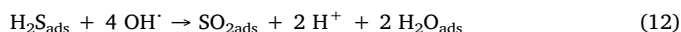
irradiation of suitable wavelength is the first step for any photocatalytic reaction (Eq. 7). Simultaneously, H_2S molecules undergo mass transfer from the bulk of the gas/solution phase to the photocatalyst and are subsequently adsorbed on its surface (Eq. 8).



Under dry conditions, $\text{H}_2\text{S}_{\text{ads}}$ molecules undergo direct oxidation via the photo-generated holes to yield sulfur (Eq. 9). The formed sulfur then reacts with the prevalent oxygen molecules to form SO_2 gas (Eq. 10) [82].



In another pathway, the surface $-\text{OH}$ groups (in the case of TiO_2 -based catalysts or other catalysts possessing a hydroxyl-rich surface) are oxidized by the photo-generated holes to yield OH^- (Eq. 11) [123]. The produced OH^- subsequently oxidize some portion of the $\text{H}_2\text{S}_{\text{ads}}$ molecules, as proposed for biogas desulfurization using a TiO_2 /zeolite (Eq. 12) [87].



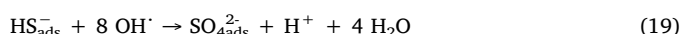
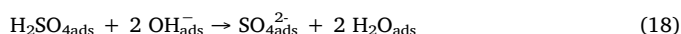
Under humid conditions, $\text{H}_2\text{S}_{\text{ads}}$ molecules can undergo direct oxidation via photo-generated holes or become hydrolyzed to yield HS_{ads}^- species, which would eventually be oxidized to sulfur through interaction with the photo-generated holes (Eqs. 13 and 14) [93].



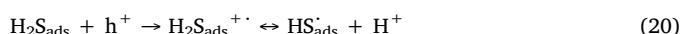
The formed sulfur could also react with OH^- to yield SO_2 gas (Eq. 15) [87].



The prime reason behind the deactivation of catalysts during photocatalytic treatment of gaseous H_2S under humid conditions has often been reported to be deposition of sulfate species on the photocatalyst surface [92]. These sulfate groups result from the oxidation of produced SO_2 by oxygen into SO_3 followed by its subsequent hydration into sulfuric acid, owing to a highly hygroscopic characteristic (Eqs. 16 and 17) [87]. The produced sulfuric acid may combine with hydroxyl ions present on the photocatalyst surface to yield sulfate functionalities (Eq. 18) [134]. The sulfate groups on the photocatalyst surface could also be produced during the direct interaction between OH^- and HS_{ads}^- species (Eq. 19) [87,193,194].



In another pathway, the $\text{H}_2\text{S}_{\text{ads}}$ molecules combine with photo-generated holes (under dry conditions) or OH^- (under humid conditions) to yield HS^\cdot , which further interacts with oxygen molecules to produce SO_2 [92] (Eqs. 20–23).



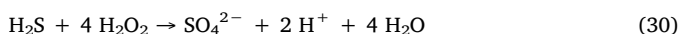
A film of water may be formed on the photocatalyst surface in the presence of excess moisture to yield free radical species that can lead to the eventual oxidation of $\text{H}_2\text{S}_{\text{ads}}$. Such reactions are encountered in aqueous phase treatment conditions (Eqs. 24–26) [134].



The application of VUV irradiation (185 nm) may promote direct photolysis of H_2S molecules to a large extent, assisting in the photocatalytic destruction process [112]. VUV irradiation promotes formation of O_3 and OH^\cdot species that can oxidize H_2S molecules to SO_2 (Eqs. 12 and 27) [104]. The formation of SO_2 should then induce the deposition of sulfate groups on the photocatalyst surface via the pathways discussed above (Eqs. 16–18).



In situ formation of H_2O_2 (through an interaction between oxygen molecules and photo-generated charge carriers) as an H_2S oxidizing agent has also been documented (Eq. 28) [131]. The generated H_2O_2 may partially or fully oxidize H_2S molecules to yield sulfur or sulfate species, which may then contribute to photocatalytic deactivation (Eqs. 29 and 30) [92,131,193,194].



Compared with conventional hydrogen production via water splitting, the splitting of H_2S in aqueous media is a more complex process and may produce several species (e.g., SO_4^{2-} , SO_2^- , S_n^{2-} , and S) in addition to hydrogen [195] (Eqs. 5, 6 and Eqs. 31–36) (Fig. 9). The splitting of H_2S is also beneficial in terms of energy requirements. However, the long-term production of hydrogen via H_2S splitting may pose a considerable challenge as the produced S_n^{2-} species are colored in nature. Their increasing accumulation in the reaction media may hinder light absorption [195]. Sulfur, generated during the process as a by-product, could deactivate the catalyst surface by blocking the active sites [156]. In contrast, $\text{S}_2\text{O}_3^{2-}$ species do not pose the above issues after long-term operation because of their optical transparency (Eq. 36). As discussed in Section 3, $\text{MnS}/(\text{In}_x\text{Cu}_{1-x})\text{S}_3$ is an effective candidate for H_2S splitting, as it can effectively desorb the formed sulfur from its surface, overcoming the drawback of frequent deactivation.

It is difficult to describe the mechanism that explains the effect of the presence/absence of humidity during the splitting of gas-phase H_2S to produce hydrogen. However, the following explanations may be used as reference. To begin, the processes under dry conditions can be described by Eq. 9. Eqs. 6, 13, and 14 describe the processes under humid conditions.



Photocatalytic reactions for H_2S removal or hydrogen production are generally inefficient and often generate several by-products or undesirable species. Future research should focus on increasing the efficiency of photocatalysis to improve overall performance in real-world domains.

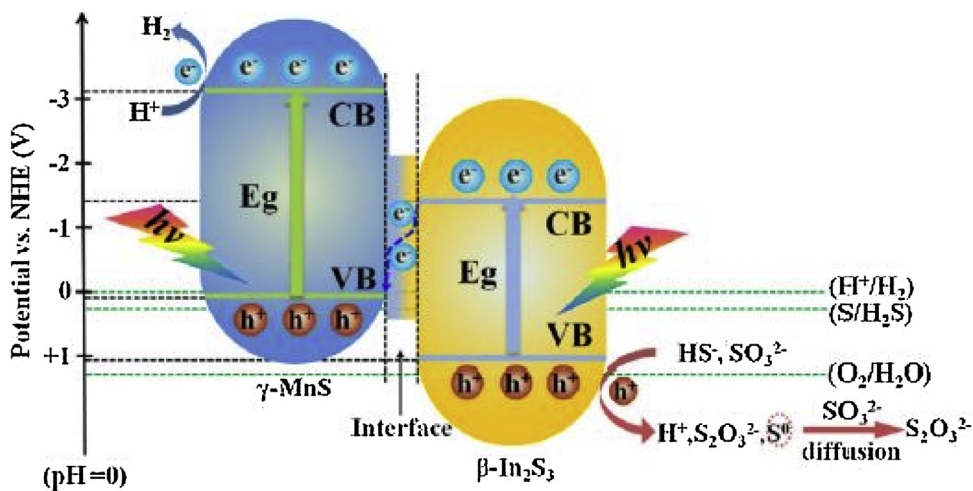


Fig. 9. Photocatalytic process of splitting H_2S by $\text{MnS}/\text{In}_2\text{S}_3$ in 0.6 M Na_2SO_3 /0.1 M $\text{Na}_2\text{S}/3\text{ M H}_2\text{S}$ solution; reproduced with permission from [158].

5. Performance comparisons of the applied photocatalytic systems

Quantitative evaluation of different photocatalysts would permit useful assessment of their performance in H_2S mineralization. The present literature provides only mineralization, conversion, or removal efficiencies under applied experimental conditions for comparison purposes, and a photocatalyst performing well under a given set of experimental conditions may not necessarily display optimal performance under varying conditions [53]. A direct comparison between different photocatalytic systems through the utilization of removal/conversion efficiency values may not allow for a meaningful comparison of actual performance. As a result, there is a pressing need for a figure-of-merit-based performance metric that takes into account all the variables associated with photocatalytic processes. We report the effective utilization of QY and SY values as critical performance metrics to gauge the actual potential of different photocatalytic systems.

Fundamentally, QY can be described as a quantitative measurement of the efficiency of a given photocatalyst to utilize the photons reaching its surface against their actual contribution to mineralizing the target analyte, i.e., kinetics and yield of photocatalysis process [196,197]. The literature provides various definitions for QY depending on the intended application [119]. For our purposes, QY values were derived using Eq. 37 [53].

$$\text{Quantum yield (QY)} = \frac{\text{Decay rate (molecules per second)}}{\text{Photon flux (photons per second)}} \quad (37)$$

As described above, QY values can be used as effective performance metrics to seek superior insights into the true photocatalytic performance compared with conversion/removal efficiency values. However, they cannot be applied directly to a comparison of multiple systems, as they do not take into account the mass of utilized photocatalysts [198]. Our comparison of SY values in conjunction with QY values allows for a judicious comparison of the performances of different photocatalytic systems, and takes into account all inherent and associated variables at the same time (Eq. 38) (Table 1).

$$\text{Space time yield (SY)} = \frac{\text{Quantum yield (molecules per photon)}}{\text{Photocatalyst mass (mg)}} \quad (38)$$

In the industrial sector, SY is described as the net amount of products produced per unit time per packed volume of the catalyst bed [199]. For our purposes, the concept of SY can be understood as the quantitative measurement of the amount of H_2S molecules mineralized per unit time by a unit mass of the photocatalyst. Owing to a lack of reported data in some cases, QY or SY values could not be computed (Table 1).

The best performance for a gas-phase photocatalytic system has been reported with a Mn-TiO_2 system, which exhibited exceptional QY and SY values of $3.76\text{E-}03$ molecules photon^{-1} and $3.75\text{E-}06$ molecules $\text{photon}^{-1} \text{ mg}^{-1}$, respectively [112] (Table 1). Besides its favorable structural/catalytic features (as elucidated in Section 2.1), the heightened photocatalytic ability of a Mn-TiO_2 system combines well with VUV irradiation to produce excellent results; UV irradiation alone could not effectively degrade H_2S molecules (a removal efficiency of 68.1%). Essentially, VUV irradiation can produce highly reactive oxygen species, such as O_3 , $\text{O}^{(1\text{D})}$, and $\text{O}^{(3\text{P})}$, to facilitate oxidation of gaseous H_2S molecules [200]. However, in the presence of Mn-TiO_2 , VUV photolysis + photocatalysis achieved an efficiency of 89.9% [112]. In addition, a TiO_2 P25 coating on the inner surface of an annular Pyrex reactor demonstrated a good QY value of $7.77\text{E-}04$ molecules photon^{-1} along with a SY value of $1.29\text{E-}06$ molecules $\text{photon}^{-1} \text{ mg}^{-1}$ [134] (Table 1). Such an approach to coating has the potential to enhance the practical applicability of many existing real-world surfaces, without requiring specialized equipment. Nevertheless, TiO_2 P25 coating exhibited optimal performance only in the absence of moisture, which could be a limitation for real-world applications [134] (Section 2.1).

A TiO_2 /zeolite composite with good performance parameters, including the ability to selectively remove H_2S from a simulated biogas, has been reported. This process was characterized with a QY value of $1.01\text{E-}04$ molecules photon^{-1} and a SY value of $5.02\text{E-}07$ molecules $\text{photon}^{-1} \text{ mg}^{-1}$ [87] (Table 1). For non- TiO_2 photocatalysts, $\text{CdS-ZnS}/\text{Fe}_2\text{O}_3$ offers optimal performance with a QY of $7.56\text{E-}06$ molecules photon^{-1} and SY of $7.55\text{E-}09$ molecules $\text{photon}^{-1} \text{ mg}^{-1}$ [144] (Table 1). As can be seen in Table 1, the literature contains few reports on gas-phase H_2S photocatalysis via non- TiO_2 catalysts. Notably, the QY and SY of the best-performing non- TiO_2 photocatalysts are remarkably lower than those of TiO_2 -based catalysts (Table 1), although these results occur under visible light. Development of a non- TiO_2 photocatalyst therefore requires further research.

As discussed earlier (Section 3), one of the most attractive features of H_2S photocatalysis is its potential to produce hydrogen gas by splitting H_2S molecules. The highest hydrogen evolution rate of $49,600 \mu\text{mol h}^{-1} \text{ g}^{-1}$ was observed in case of $\text{MnS}/\text{In}_2\text{S}_3\text{-MoS}_2$ [164] (Table 2). Such enhanced performance may be ascribable to the effective separation of photo generated charge carriers through the establishment of an internal electric field between MnS and MoS_2 . (Here, work functions of 5.074 and 5.087 eV were noted for MoS_2 and MnS , respectively.) Interestingly, $\text{Cu}_2\text{S}/\text{TiO}_2$ core-shell particles also displayed good hydrogen evolution rate of $41,600 \mu\text{mol h}^{-1} \text{ g}^{-1}$ [174] (Table 2). Their enhanced performance was accounted for by the effective resistance of Cu_2S against photo corrosion and charge carrier separation through the formation of an effective core-shell structure

Table 3Performance table for continuous-mode adsorption systems applied for the removal of gaseous H₂S.

Order	Adsorbent	Sorbent mass (mg)	Concentration (ppm)	Operation time (h)	Capacity (mg g ⁻¹)	Space velocity (h ⁻¹)	Estimated cost (USD g ⁻¹)	Reference
1	Activated carbon	5	10	0.05	0.11	2.20E-03	0.006	[205,215]
2	Carbopack-X	5	10	0.02	0.05	2.86E-03	0.06	[205,215]
3	MOF-199	5	10	14.4	69	4.80E-03	15	[205,215]
4	MOF-5	5	10	1.8	4.97	2.72E-03	9 (for the organic linker only)	[215,216]
5	UiO-66-NH ₂	5	10	0.025	0.07	2.80E-03	4.77 (for the organic linker only)	[215,216]

[174]. An appreciable hydrogen evolution rate of 29,705 μmol h⁻¹ g⁻¹ was observed for N-TiO₂/Gr [189] (Table 2). Its performance may be associated with the enhanced charge carrier mobility due possibly to the co-presence of graphene. Additionally, nitrogen doping of TiO₂ was potentially effective option in enhancing the solar light absorption capability of the photocatalyst [189]. MnS/(In_xCu_{1-x})₂S₃ and MnS/In₂S₃/PdS also displayed good hydrogen production rates of 29,252 and 22,700 μmol h⁻¹ g⁻¹, respectively [156,168] (Table 2). The enhanced performances of these composites can be attributed to their ability to desorb the produced sulfur from their surfaces, as it was efficient to avoid deactivation. Moreover, the unique structures of MnS/(In_xCu_{1-x})₂S₃ and MnS/In₂S₃/PdS enabled the efficient absorption of photons, even in the visible light regime, while beneficial in amplifying the separation of photo-generated charge carriers [156,168] (refer to Section 3). The low hydrogen evolution rate of 6.5E-04 μmol h⁻¹ g⁻¹ seen by CdS-ZnS/Fe₂O₃ indicates that gas-phase production of hydrogen via H₂S splitting may proceed relatively inefficiently. This is the only recent report made for the direct gas-phase splitting of H₂S for hydrogen production in the literature [144] (Table 2). All reported studies on hydrogen production via photocatalytic splitting of H₂S were conducted under visible or solar light. As such, the photocatalytic technology for H₂S splitting aimed towards hydrogen production can possibly be implemented for real-world applications if operated efficiently under solar irradiation (Table 2).

At present, adsorption is one of the most common strategies being employed to capture gaseous H₂S [11,32,33]. Nevertheless, as spent sorbent requires frequent regeneration, the practical utility of adsorption is limited [63]. Also, the most powerful adsorbents for sulfurous species (e.g., metal-organic frameworks [MOFs] and other chemically modified/functionalized materials) preferentially capture H₂S molecules via chemisorption to disable regeneration of the sorbent (e.g., through structural collapse of frameworks and/or the chemical transformation of the H₂S molecules) [32,33,201,202]. In contrast, a photocatalytic approach can be used to destroy a wide range of pollutants [61,86]. As a consequence, photocatalysts are being investigated as prospective alternatives to conventional adsorption technology. A direct comparison of the performances of photocatalytic and adsorption systems is often unfeasible as they involve inherently different mechanisms and operational variables. However, quantitative assessment and performance comparisons are useful for existing technologies [203]. We recently proposed applying the space velocity concept to a comparison of gas-phase continuous-mode treatment systems [203]. Below we present the definition and meaning of space velocity and describe its application for practical comparison purposes to gaseous H₂S treatment.

Although the overall mechanisms of gas-phase photocatalysis and adsorption are inherently different, they share some physicochemical processes and goals during removal of a target analyte. For the gas-phase continuous-mode operation, both systems consist of a photocatalyst/adsorbent bed over which the influent stream laden with target species is passed to reduce pollutant concentrations. A common performance metric (e.g., space velocity) could be utilized to compare the performances of adsorption and photocatalytic systems based on their physicochemical similarities. The concept of space velocity is primarily

based on chemical and industrial engineering principles. In the field of chemical engineering, the space velocity of a process reactor is defined as the amount of equivalent reactor volumes of the gaseous influent that can be processed in an unit time interval [204] (Eq. 39).

Space velocity (h⁻¹)

$$= \frac{\text{Flow rate (L h}^{-1}\text{)} \times (\text{Inlet} - \text{Outlet pollutant concentration (mg L}^{-1}\text{)})}{\text{Adsorbent or photocatalyst mass (mg)}} \quad (39)$$

Space velocity values for continuous-mode photocatalytic systems with H₂S as a gas-phase target are summarized in Table 1. For comparative purposes, the values for some representative gas-phase adsorbents that remove H₂S under continuous mode are presented in Table 3. In general, photocatalytic systems performed on par with or sometimes better than the adsorption systems. The highest space velocity was seen in a Mn-TiO₂ system utilizing VUV irradiation (1.12E-02 h⁻¹), which was about 2.3 times higher than the highest value associated with adsorption of H₂S by MOF-199 (4.8E-03 h⁻¹) (Tables 1 and 3). Some other photocatalytic systems utilizing TiO₂ P25 coating (1.11E-02 h⁻¹) and TiO₂/zeolite (7.51E-03 h⁻¹) outperformed the adsorption systems (Tables 1 and 3). However, those seemingly superior performances may not represent true ascendancy over adsorption systems. A common breakthrough limit or conversion percentage for both systems must be defined to obtain a truly meaningful comparison. For gas-phase continuous-mode systems (photocatalysis or adsorption), the pollutant concentration rises steadily at the sorbent/catalyst bed outlet in accordance with the breakthrough profile (as seen from adsorptive/photocatalytic removal) of the material [205]. Because reports on gas-phase continuous-mode photocatalysis rarely present full-scale breakthrough profiles, it is not possible to extract sufficient data to match a breakthrough concept for photocatalysis in parallel with adsorptive processes. Space velocity values for adsorption systems were calculated at the 100% breakthrough point, i.e., when the sorbent bed outlet pollutant concentration becomes approximately equal to that at the sorbent bed inlet (Table 3). On the contrary, the reported data for photocatalytic systems are highly restrictive and the performance data are only presented up to high conversion values (e.g., 80–90%) and do not present full breakthrough (Table 1). Publication of full breakthrough profiles of continuous-mode photocatalytic systems would enable more meaningful evaluation of the corresponding adsorption systems.

The space velocity approach could be applied to gauge true performance comparisons by setting a specific breakthrough point. Still, the space velocity values in this review article clearly show that for practical gaseous H₂S removal, the photocatalytic approach holds great promise, at least in terms of removal performance. Additionally, since inexpensive sorbents (e.g., activated carbon) show little affinity toward H₂S, expensive materials such as MOFs are necessary [32,33] (Table 3). TiO₂ is a relatively abundant and low-cost material, and the lab-scale success of TiO₂-based photocatalysts in gaseous H₂S treatment offers great promise. However, the need for a suitable light source, rapid deactivation, diminished performance under real-world conditions, and production of harmful intermediate by-products (e.g., SO₂ in the case of H₂S treatment) raises questions regarding the potential applicability of

photocatalysis under harsh practical conditions [65]. Some researchers have suggested using integrated adsorption-photocatalytic systems to control the emission of toxic by-products and improve overall target removal efficiency [65,86].

6. Challenges in photocatalyst-based approaches for H₂S removal and hydrogen production

The main goal of utilizing photocatalytic technology is to remove hazardous compounds (e.g., H₂S) from the air. The primary attraction of the photocatalytic approach is the possibility of completely mineralizing a target pollutant rather than simply transferring it from one phase to another via chemical interactions. In spite of some optimistic results in lab-scale models, the applicability of photocatalytic technology to air quality management remains a challenge because of multiples limitations and technological shortcomings under real-world conditions.

6.1. Production of hazardous intermediates/by-products

The primary advantage of photocatalytic technology is its ability to transform target pollutants into less-toxic end products. Nevertheless, photocatalytic reactions often involve multiple pathways that eventually result in the accumulation of unintended hazardous compounds. In certain cases, the formed intermediates are even more toxic than the parent compound (e.g., aldehydes formed during the photocatalytic destruction of gaseous benzene) [80]. The formation of hazardous SO_x species (e.g., SO₂ and SO₃) during the photocatalytic treatment of H₂S-laden air is its most serious drawback. SO₂ is toxic, corrosive, and odorous, and it is listed as a prime environmental target by the United States Environmental Protection Agency [206,207]. Moreover, SO_x species are primarily responsible for the formation of acid rain [208,209]. As a consequence, photocatalytic treatment of H₂S-rich air can pose a significant threat from an environmental and health perspective. Further research efforts should be directed toward engineering efficient photocatalysts that avoid the formation or liberation of toxic species like SO_x. For example, a photocatalyst system may be integrated with a SO_x-selective sorbent bed (e.g., oxidized/modified carbon materials and metal oxides) [210–212]. However, such a system would add to the complexity and operational costs [65,86].

6.2. Rapid deactivation of the photocatalyst

Considerable decline in overall removal performance is inevitable as a photocatalytic deactivation process advances. Moreover, photocatalytic deactivation leads to a significant rise in by-product or intermediate product concentration due to incomplete mineralization of target analytes. On the other hand, a short operating period/lifespan may lead to high operating costs and the process may need frequent catalyst regeneration/replacement [65]. Photocatalytic deactivation is caused primarily by the recombination of e⁻-h⁺ pairs along with the deposition of non-volatile and highly stable intermediate compounds (e.g., sulfate and sulfur deposits in case of H₂S). The deposition of stable intermediates on a photocatalyst surface blocks reaction sites while enhancing catalytic photo-corrosion. The regeneration of a spent photocatalyst can be carried out by subjecting it to UV irradiation, temperature rise, or fresh air [92,131]. However, in cases where photocatalytic deactivation is due to sulfate deposits (as in H₂S photocatalysis), regeneration is only possible through specific chemical treatments (e.g., calcination and washing with weak base) [87,92] (refer to Section 2.1). Such techniques can be unwieldy and inefficient. Further insights into the mechanism of H₂S photocatalysis and subsequent deactivation would help researchers enhance overall performance with respect to real-world applications.

6.3. Lack of studies on H₂S splitting and experimental data

H₂S splitting provides a sustainable route to the production of an energy carrier in the form of hydrogen while allowing simultaneous management of H₂S. However, as the literature has little to say on this subject, it is difficult to describe the aspects of such a process (Table 2). Photocatalytic H₂S splitting is often limited by the swift deposition of sulfur on a catalyst surface, and the need to regenerate or replace the catalyst complicates the process. Although ingeniously designed photocatalysts have been reported with in situ capability of rejecting sulfur from their surfaces (e.g., MnS/(In_xCu_{1-x})₂S₃), efficiency rates under practical conditions remain unknown [156]. Also, H₂S splitting processes often lead to side reactions and the accumulation of by-product sulfur species (e.g., SO₄²⁻, SO₂, S_n²⁻, and S) that tend to aggravate photocatalytic deactivation and lower overall efficiency [195].

The generation of S_n²⁻ species (colored in nature) significantly hinders light penetration in aqueous solutions, reducing photocatalytic performance [195]. If photocatalytic H₂S splitting can be engineered to produce S₂O₃²⁻ species in place of S_n²⁻ species, long-term operation of such a process may be possible (refer to Sections 3 and 4). Moreover, the effect of solution pH on hydrogen production via H₂S splitting is poorly understood [184], and little attention has been paid to direct gas-phase photocatalytic H₂S splitting for hydrogen production [144] (Table 2). At present, H₂S-laden air is bubbled through an aqueous suspension of a photocatalyst, leading to the evolution of hydrogen gas. However, such systems require additional pumping and pH maintenance, which can add to operational costs and complexity. Further research efforts should be devoted to a better understanding the photocatalytic H₂S splitting mechanisms and amplifying the performance of gas-phase H₂S splitting systems to avoid unnecessary operational and maintenance costs.

Most photocatalytic experiments involve laboratory-scale models operating under unrealistic conditions (e.g., low humidity levels and/or large catalyst mass). Most studies on photocatalytic removal of gaseous H₂S have been conducted using TiO₂-based catalysts that operate only under UV illumination (Table 1). Such a system would consume large amounts of energy, making practical application unrealistic [65,213]. Further research efforts should focus on synthesizing novel photocatalysts capable of operating under visible or solar irradiation. The use of lab-scale experiments are warranted from a research perspective, but there is a pressing need to propel photocatalytic technology into the field and validate its efficacy under harsh real-world conditions [65,213]. Additionally, as discussed earlier (Section 5), the published literature on gas-phase continuous-mode H₂S photocatalytic systems does not include a complete breakthrough profile for the process. Elucidation of the complete catalytic reaction would produce data sets comparable to a breakthrough profile of adsorption processes and allow for an assessment of the true performance of a given photocatalytic system (Section 5).

7. Conclusions and future prospects

The present article examined recent scientific developments in the field of photocatalytic treatment of gaseous odorants (e.g., H₂S). Recent years have witnessed a prolific rise in endeavors associated with the photocatalytic technology in light of its most promising feature — complete mineralization of target pollutants. To facilitate an in-depth discussion on applied photocatalysts for gaseous H₂S, all available options were subdivided into TiO₂ and non-TiO₂-based catalysts. The quantitative performance of various photocatalysts was then assessed in terms quantum and space-time yields, coupled with their inherent features (surface chemistry, structure, and functionality) and prevailing operational factors (moisture content, regenerability, and type of light source). Theoretically, the presence of relative humidity in the system should amplify photocatalytic performance owing to the generation of large quantities of hydroxyl radicals. However, experimental

observations indicate that the sorption of target molecules onto a photocatalyst is inhibited under excess levels of moisture due to competitive effects to reduce the performance. It is therefore important to determine the optimal relative humidity for a photocatalyst.

Photocatalysts based on TiO_2 have received considerable attention owing to their abundance, non-toxicity, low cost, and chemical stability. Nevertheless, their apparent shortcomings (swift deactivation, quick recombination of photo-generated charge carriers, operational capability only under UV irradiation, and low quantum efficiency) have propelled the development of non- TiO_2 photocatalysts capable of operating under visible light or solar irradiation. Several novel strategies (such as doping the parent TiO_2 structure with metals/nonmetals, combining them with suitable support materials, and synthesizing heterojunctions) have been validated to help upgrade the performance of TiO_2 -based photocatalysts.

One of the most attractive features of H_2S photocatalysis is the splitting of parent molecules to yield hydrogen as a main product. H_2S splitting theoretically provides a win-win strategy, as it reduces the concentrations of hazardous substances while simultaneously providing a clean energy carrier. However, studies on this topic are few in number, and future research on H_2S photocatalysis should be conducted to uncover the potential of H_2S splitting for hydrogen production. Furthermore, an entire section was dedicated to understanding the prevailing mechanisms involved in photocatalytic H_2S removal and hydrogen production via H_2S splitting. Attempts were made to quantitatively compare the performances of various photocatalytic systems in terms of quantum and space-time yields. The concept of space velocity was proposed as a viable platform to directly compare the performances of gas-phase adsorption and photocatalysis operated in continuous mode. Despite enormous efforts in this area, experimental data that would permit assessments of photocatalytic performance under real-world conditions are lacking. To shift this technology from the lab to the real world, chemists, environmental engineers, and material scientists should collaborate in this interesting, challenging, and promising field.

Declaration of Competing Interest

The authors declare that they have no known competing financial interests or personal relationships that could have appeared to influence the work reported in this paper.

Acknowledgments

The authors acknowledge the support of the R&D Center for Green Patrol Technologies through the R&D for Global Top Environmental Technologies funded by the Ministry of Environment (MOE 2018001850001) as well as a grant from the National Research Foundation of Korea funded by the Ministry of Science, ICT & Future Planning (Grant No: 2016R1E1A1A01940995).

References

- [1] P. Agarwal, M. Sarkar, B. Chakraborty, T. Banerjee, Chapter 7 - Phytoremediation of air pollutants: prospects and challenges, in: V.C. Pandey, K. Baudh (Eds.), *Phytomanagement of Polluted Sites*, Elsevier, 2019, pp. 221–241.
- [2] L. Yang, L. Yang, L. Ding, F. Deng, X.-B. Luo, S.-L. Luo, 1 - Principles for the application of nanomaterials in environmental pollution control and resource reutilization, in: X. Luo, F. Deng (Eds.), *Nanomaterials for the Removal of Pollutants and Resource Reutilization*, Elsevier, 2019, pp. 1–23.
- [3] Z. Li, D. Li, L. Wang, C. Lu, P. Shan, X. Zou, Z. Li, Photocontrollable water-soluble polymeric hydrogen sulfide (H_2S) donor, *Polymer* 168 (2019) 16–20.
- [4] K. Vikrant, V. Kumar, Y.S. Ok, K.-H. Kim, A. Deep, Metal-organic framework (MOF)-based advanced sensing platforms for the detection of hydrogen sulfide, *Trac Trends Anal. Chem.* 105 (2018) 263–281.
- [5] K.-H. Kim, A. Adelodun, A. Deep, E. Kwon, E.-C. Jeon, Y.-H. Kim, S.-H. Jo, M.-H. Lee, S.-B. Cho, O.-H. Hwang, Performance of air fresher system for the removal of various odorants released from foodstuffs, *Asian J. Atmos. Environ.* 11 (2017) 37–53.
- [6] K. Vikrant, S.K. Kailasa, D.C.W. Tsang, S.S. Lee, P. Kumar, B.S. Giri, R.S. Singh, K.-H. Kim, Biofiltration of hydrogen sulfide: trends and challenges, *J. Clean. Prod.* 187 (2018) 131–147.
- [7] J. Zhang, R. Sokolovskij, G. Chen, Y. Zhu, Y. Qi, X. Lin, W. Li, G.Q. Zhang, Y.-L. Jiang, H. Yu, Impact of high temperature H_2 pre-treatment on Pt-AlGaN/GaN HEMT sensor for H_2S detection, *Sens. Actuators B Chem.* 280 (2019) 138–143.
- [8] X. Dong, Y. Su, T. Lu, L. Zhang, L. Wu, Y. Lv, MOFs-derived dodecahedr porous Co_3O_4 : an efficient cataluminiscence sensing material for H_2S , *Sens. Actuators B Chem.* 258 (2018) 349–357.
- [9] J. Jiang, A. Chan, S. Ali, A. Saha, K.J. Haushalter, W.-L.M. Lam, M. Glasheen, J. Parker, M. Brenner, S.B. Mahon, H.H. Patel, R. Ambasudhan, S.A. Lipton, R.B. Pilz, G.R. Boss, Hydrogen sulfide—mechanisms of toxicity and development of an antidote, *Sci. Rep.* 6 (2016) 20831.
- [10] G. Yue, D. Huang, F. Luo, L. Guo, B. Qiu, Z. Lin, G. Chen, Highly selective fluorescence sensor for hydrogen sulfide based on the Cu(II)-dependent DNAzyme, *J. Lumin.* 207 (2019) 369–373.
- [11] Z. Aslam, I.A. Hussein, R.A. Shawabkeh, M.A. Parvez, W. Ahmad, Ihsanullah, Adsorption kinetics and modeling of H_2S by treated waste oil fly ash, *J. Air Waste Manage. Assoc.* 69 (2019) 246–257.
- [12] K. Ge, Y. Wu, T. Wang, J. Wu, Humidity swing adsorption of H_2S by fibrous polymeric ionic liquids (PILs), *Sep. Purif. Technol.* 217 (2019) 1–7.
- [13] A. Peluso, N. Gargiulo, P. Aprea, F. Pepe, D. Caputo, Nanoporous materials as H_2S adsorbents for biogas purification: a review, *Sep. Purif. Rev.* 48 (2019) 78–89.
- [14] A. Adelodun, K. Vellingiri, B.-H. Jeon, J.-M. Oh, S. Kumar, K.-H. Kim, A test of relative removal properties of various offensive odors by zeolite, *Asian J. Atmos. Environ.* 11 (2017) 15–28.
- [15] P. San-Valero, J.M. Penya-roja, F. Javier Álvarez-Hornos, G. Buitrón, C. Gabaldón, G. Quijano, Fully aerobic bioscrubber for the desulfurization of H_2S -rich biogas, *Fuel* 241 (2019) 884–891.
- [16] A. Singh, V. Pandey, R. Bagai, M. Kumar, J. Christopher, G.S. Kapur, ZnO-decorated MWCNTs as solvent free nano-scrubber for efficient H_2S removal, *Mater. Lett.* 234 (2019) 172–174.
- [17] H. Abdolahi-Mansoorkhani, S. Seddighi, H_2S and CO_2 capture from gaseous fuels using nanoparticle membrane, *Energy* 168 (2019) 847–857.
- [18] S.M. Mirfendereski, Z. Niazi, T. Mohammadi, Selective removal of H_2S from gas streams with high CO_2 concentration using hollow-fiber membrane contractors, *Chem. Eng. Technol.* 42 (2019) 196–208.
- [19] M. Dan, A. Prakash, Q. Cai, J. Xiang, Y. Ye, Y. Li, S. Yu, Y. Lin, Y. Zhou, Energy-band-Controlling strategy to construct novel $\text{Cd}x\text{In}_{1-x}\text{S}$ solid solution for durable visible light photocatalytic hydrogen sulfide splitting, *Solar RRL* 3 (2019) 1800237.
- [20] M. Lashgari, M. Ghanimati, A new efficient eco-friendly quaternary solid-solution nanoenergy material for photocatalytic hydrogen fuel production from H_2S aqueous feed, *Chem. Eng. J.* 358 (2019) 153–159.
- [21] N. Raza, K.-H. Kim, H. Agbe, S.K. Kailasa, J. Szulejko, R. Brown, Recent advances in titania-based composites for photocatalytic degradation of indoor volatile organic compounds, *Asian J. Atmos. Environ.* 11 (2017) 217–234.
- [22] P.V.L. Reddy, K.-H. Kim, Y.-H. Kim, A review of photocatalytic treatment for various air pollutants, *Asian J. Atmos. Environ.* 5 (2011) 181–188.
- [23] Y. Chen, L. Xie, W. Cai, J. Wu, Pilot-scale study using biotrickling filter to remove H_2S from sewage lift station: experiment and CFD simulation, *Biochem. Eng. J.* 144 (2019) 177–184.
- [24] K. Vikrant, K.-H. Kim, J.E. Szulejko, S.K. Pandey, R.S. Singh, B.S. Giri, R.J.C. Brown, S.H. Lee, Bio-filters for the treatment of VOCs and odors, *Asian J. Atmos. Environ.* 11 (2017) 139–152.
- [25] D. Barba, F. Cammarota, V. Vaiano, E. Salzano, V. Palma, Experimental and numerical analysis of the oxidative decomposition of H_2S , *Fuel* 198 (2017) 68–75.
- [26] X. Wang, W. Zhang, Q. Gao, Y. Wang, J. Zhang, J. Zhou, Q. Liu, G. Qian, A critical role of benzoquinone basic group in catalytic oxidation of H_2S by sewage sludge-derived catalyst, *Appl. Surf. Sci.* 470 (2019) 1010–1017.
- [27] V. Irani, A. Tavasoli, M. Vahidi, Preparation of amine functionalized reduced graphene oxide/methyl diethanolamine nanofluid and its application for improving the CO_2 and H_2S absorption, *J. Colloid Interface Sci.* 527 (2018) 57–67.
- [28] A. Singh, Y. Sharma, Y. Wupardarasta, K. Desai, Selection of amine combination for CO_2 capture in a packed bed scrubber, *Resour. Technol.* 2 (2016) S165–S170.
- [29] F. Shakerian, K.-H. Kim, J.E. Szulejko, J.-W. Park, A comparative review between amines and ammonia as sorptive media for post-combustion CO_2 capture, *Appl. Energy* 148 (2015) 10–22.
- [30] S. Mokhatab, W.A. Poe, J.Y. Mak, Chapter 7 - Natural gas treating, in: S. Mokhatab, W.A. Poe, J.Y. Mak (Eds.), *Handbook of Natural Gas Transmission and Processing*, fourth edition, Gulf Professional Publishing, 2019, pp. 231–269.
- [31] G. Coppola, D. Papurello, Biogas cleaning: activated carbon regeneration for H_2S removal, *Clean Technol.* 1 (2018).
- [32] Y. Deng, K. Vellingiri, K.-H. Kim, D.W. Boukhvalov, L. Philip, Activation strategies of metal-organic frameworks for the sorption of reduced sulfur compounds, *Chem. Eng. J.* 350 (2018) 747–756.
- [33] K. Vellingiri, A. Deep, K.-H. Kim, Metal-Organic frameworks as a potential platform for selective treatment of gaseous sulfur compounds, *ACS Appl. Mater. Interfaces* 8 (2016) 29835–29857.
- [34] T.J. Bandosz, A. Bagreev, F. Adib, A. Turk, Unmodified versus caustics-impregnated carbons for control of hydrogen sulfide emissions from sewage treatment plants, *Environ. Sci. Technol.* 34 (2000) 1069–1074.
- [35] R. Sitthikhankhaew, S. Predapitakkun, R. Kiattikomol, S. Pumhiran, S. Assabumrungrat, N. Laosiripojana, Comparative study of hydrogen sulfide adsorption by using alkaline impregnated activated carbons for hot fuel gas purification, *Energy Procedia* 9 (2011) 15–24.

[36] T.J. Bandosz, Effect of pore structure and surface chemistry of virgin activated carbons on removal of hydrogen sulfide, *Carbon* 37 (1999) 483–491.

[37] T.J. Bandosz, Q. Le, Evaluation of surface properties of exhausted carbons used as H₂S adsorbents in sewage treatment plants, *Carbon* 36 (1998) 39–44.

[38] R.W. Baker, K. Lokhandwala, Natural gas processing with membranes: an overview, *Ind. Eng. Chem. Res.* 47 (2008) 2109–2121.

[39] A. Tabe-Mohammadi, A review of the applications of membrane separation technology in natural gas treatment, *Sep. Sci. Technol.* 34 (1999) 2095–2111.

[40] C.A. Scholes, G.W. Stevens, S.E. Kentish, The effect of hydrogen sulfide, carbon monoxide and water on the performance of a PDMS membrane in carbon dioxide/nitrogen separation, *J. Memb. Sci.* 350 (2010) 189–199.

[41] M. Ben Jaber, A. Couvert, A. Amrane, F. Rouxel, P. Le Cloirec, E. Dumont, Biofiltration of high concentration of H₂S in waste air under extreme acidic conditions, *N. Biotechnol.* 33 (2016) 136–143.

[42] M.B. Jaber, B. Anet, A. Amrane, C. Couriol, T. Lendormi, P.L. Cloirec, G. Cogny, R. Fillières, Impact of nutrients supply and pH changes on the elimination of hydrogen sulfide, dimethyl disulfide and ethanethiol by biofiltration, *Chem. Eng. J.* 258 (2014) 420–426.

[43] S. Gerrity, C. Kennedy, E. Clifford, G. Collins, Hydrogen sulfide oxidation in novel Horizontal-Flow Biofilm Reactors dominated by an Acidithiobacillus and a Thiobacillus species, *Environ. Technol.* 37 (2016) 2252–2264.

[44] K.A. Rabbani, W. Charles, A. Kayaalp, R. Cord-Ruwisch, G. Ho, Biofilter for generation of concentrated sulphuric acid from H₂S, *Environ. Sci. Pollut. Res.* 23 (2016) 16781–16789.

[45] J.S. Eow, Recovery of sulfur from sour acid gas: a review of the technology, *Environ. Prog.* 21 (2002) 143–162.

[46] A. Bahadori, Chapter 11 - Sulfur recovery, in: A. Bahadori (Ed.), *Natural Gas Processing*, Gulf Professional Publishing, Boston, 2014, pp. 519–546.

[47] J.G. Speight, Chapter 7 - Processes, in: J.G. Speight (Ed.), *Natural Gas*, Gulf Publishing Company, 2007, pp. 161–192.

[48] H.A. Long, T. Wang, 16 - A simulated IGCC case study without CCS, in: T. Wang, G. Stiegel (Eds.), *Integrated Gasification Combined Cycle (IGCC) Technologies*, Woodhead Publishing, 2017, pp. 643–663.

[49] A. Taghizadeh Damanabi, F. Bahadori, A new approach for hydrogen production in Claus sulfur recovery process, *J. Sulfur Chem.* 40 (2019) 137–148.

[50] S.V. Tambwekar, M. Subrahmanyam, Photocatalytic generation of hydrogen from hydrogen sulfide: an energy bargain, *Int. J. Hydrogen Energy* 22 (1997) 959–965.

[51] S. Mokhatab, W.A. Poe, J.Y. Mak, Chapter 8 - Sulfur recovery and handling, in: S. Mokhatab, W.A. Poe, J.Y. Mak (Eds.), *Handbook of Natural Gas Transmission and Processing*, fourth edition, Gulf Professional Publishing, 2019, pp. 271–305.

[52] S. Yu, Y. Zhou, Photochemical Decomposition of Hydrogen Sulfide, *Advanced Catalytic Materials - Photocatalysis and Other Current Trends*, IntechOpen, London, United Kingdom, 2016.

[53] H. Anwer, A. Mahmood, J. Lee, K.-H. Kim, J.-W. Park, A.C.K. Yip, Photocatalysts for degradation of dyes in industrial effluents: opportunities and challenges, *Nano Res.* (2019).

[54] M. Schreck, M. Niederberger, Photocatalytic gas phase reactions, *Chem. Mater.* 31 (2019) 597–618.

[55] J. Wu, J. Ren, W. Pan, P. Lu, Y. Qi, Modified photocatalysts, in: J. Wu, J. Ren, W. Pan, P. Lu, Y. Qi (Eds.), *Photo-Catalytic Control Technologies of Flue Gas Pollutants*, Springer, Singapore, Singapore, 2019, pp. 65–82.

[56] L. Guo, Y. Chen, J. Su, M. Liu, Y. Liu, Obstacles of solar-powered photocatalytic water splitting for hydrogen production: a perspective from energy flow and mass flow, *Energy* 172 (2019) 1079–1086.

[57] T. Takata, K. Domen, Particulate photocatalysts for water splitting: recent advances and future prospects, *ACS Energy Lett.* 4 (2019) 542–549.

[58] Z. Wang, C. Li, K. Domen, Recent developments in heterogeneous photocatalysts for solar-driven overall water splitting, *Chem. Soc. Rev.* (2019).

[59] U.V. Kawade, R.P. Panmand, Y.A. Sethi, M.V. Kulkarni, S.K. Apte, S.D. Naik, B.B. Kale, Environmentally benign enhanced hydrogen production via lethal H₂S under natural sunlight using hierarchical nanostructured bismuth sulfide, *RSC Adv.* 4 (2014) 49295–49302.

[60] D.L. Maurer, J.A. Koziel, On-farm pilot-scale testing of black ultraviolet light and photocatalytic coating for mitigation of odor, odorous VOCs, and greenhouse gases, *Chemosphere* 221 (2019) 778–784.

[61] Z. Shayegan, C.-S. Lee, F. Haghightat, TiO₂ photocatalyst for removal of volatile organic compounds in gas phase – a review, *Chem. Eng. J.* 334 (2018) 2408–2439.

[62] M. Wen, G. Li, H. Liu, J. Chen, T. An, H. Yamashita, Metal–organic framework-based nanomaterials for adsorption and photocatalytic degradation of gaseous pollutants: recent progress and challenges, *Environ. Sci. Nano* (2019).

[63] T. Dutta, T. Kim, K. Vellingiri, D.C.W. Tsang, J.R. Shon, K.-H. Kim, S. Kumar, Recycling and regeneration of carbonaceous and porous materials through thermal or solvent treatment, *Chem. Eng. J.* 364 (2019) 514–529.

[64] R.B.P. Marcelino, C.C. Amorim, Towards visible-light photocatalysis for environmental applications: band-gap engineering versus photons absorption—a review, *Environ. Sci. Pollut. Res.* 26 (2019) 4155–4170.

[65] P. Pichat, A brief survey of the practicality of using photocatalysis to purify the ambient air (indoors or outdoors) or air effluents, *Appl. Catal. B Environ.* 245 (2019) 770–776.

[66] N. Shehzad, M. Tahir, K. Johari, T. Murugesan, M. Hussain, A critical review on TiO₂ based photocatalytic CO₂ reduction system: strategies to improve efficiency, *J. Co₂ Util.* 26 (2018) 98–122.

[67] T. Di, Q. Xu, W. Ho, H. Tang, Q. Xiang, J. Yu, Review on metal sulphide-based Z-scheme photocatalysts, *ChemCatChem* 11 (2019) 1394–1411.

[68] C.V. Reddy, K.R. Reddy, N.P. Shetti, J. Shim, T.M. Aminabhavi, D.D. Dionysiou, Hetero-nanostructured metal oxide-based hybrid photocatalysts for enhanced photoelectrochemical water splitting – a review, *Int. J. Hydrogen Energy* (2019).

[69] A.H. Mamaghani, F. Haghightat, C.-S. Lee, Photocatalytic degradation of VOCs on various commercial titanium dioxides: impact of operating parameters on removal efficiency and by-products generation, *Build. Environ.* 138 (2018) 275–282.

[70] A.H. Mamaghani, F. Haghightat, C.-S. Lee, Gas phase adsorption of volatile organic compounds onto titanium dioxide photocatalysts, *Chem. Eng. J.* 337 (2018) 60–73.

[71] T. Simon, M.T. Carlson, J.K. Stolarsky, J. Feldmann, Electron transfer rate vs recombination losses in photocatalytic H₂ generation on Pt-Decorated CdS nanorods, *ACS Energy Lett.* 1 (2016) 1137–1142.

[72] S. Zhu, D. Wang, Photocatalysis: basic principles, diverse forms of implementations and emerging scientific opportunities, *Adv. Energy Mater.* 7 (2017) 1700841.

[73] T. Gershon, B. Shin, N. Bojarczuk, M. Hopstaken, D.B. Mitzi, S. Guha, The role of sodium as a surfactant and suppressor of non-radiative recombination at internal surfaces in Cu₂ZnSnS₄, *Adv. Energy Mater.* 5 (2015) 1400849.

[74] F.A. Sofi, K. Majid, Enhancement of the photocatalytic performance and thermal stability of an iron based metal–organic-framework functionalised by Ag/Ag₃PO₄, *Mater. Chem. Front.* 2 (2018) 942–951.

[75] R. Qin, F. Meng, M.W. Khan, B. Yu, H. Li, Z. Fan, J. Gong, Fabrication and enhanced photocatalytic property of TiO₂-ZnO composite photocatalysts, *Mater. Lett.* 240 (2019) 84–87.

[76] M.T. Noman, M.A. Ashraf, A. Ali, Synthesis and applications of nano-TiO₂: a review, *Environ. Sci. Pollut. Res.* 26 (2019) 3262–3291.

[77] C. Prasad, H. Tang, I. Bahadur, Graphitic carbon nitride based ternary nanocomposites: from synthesis to their applications in photocatalysis: a recent review, *J. Mol. Liq.* 281 (2019) 634–654.

[78] V. Binas, D. Venieri, D. Kotzias, G. Kiriakidis, Modified TiO₂ based photocatalysts for improved air and health quality, *J. Mater.* 3 (2017) 3–16.

[79] M. Malayeri, F. Haghightat, C.-S. Lee, Modeling of volatile organic compounds degradation by photocatalytic oxidation reactor in indoor air: a review, *Build. Environ.* (2019).

[80] A.H. Mamaghani, F. Haghightat, C.-S. Lee, Photocatalytic oxidation technology for indoor environment air purification: the state-of-the-art, *Appl. Catal. B Environ.* 203 (2017) 247–269.

[81] A. Alonso-Tellez, D. Robert, V. Keller, N. Keller, H₂S photocatalytic oxidation over WO₃/TiO₂ hombikat UV100, *Environ. Sci. Pollut. Res.* 21 (2014) 3503–3514.

[82] R. Portela, M.C. Canelas, B. Sánchez, F.C. Marques, A.M. Stumbo, R.F. Tessimari, J.M. Coronado, S. Suárez, H₂S photodegradation by TiO₂/M-MCM-41 (M = Cr or Ce): deactivation and by-product generation under UV-A and visible light, *Appl. Catal. B Environ.* 84 (2008) 643–650.

[83] C. Venkata Reddy, K.R. Reddy, N.P. Shetti, A. Mishra, S. Basu, Chapter 30 - Recent progress in TiO₂- and ZnO-based nanostructured hybrid photocatalysts for water purification and hydrogen generation, in: S. Thomas, D. Pasquini, S.-Y. Leu, D.A. Gopakumar (Eds.), *Nanoscale Materials in Water Purification*, Elsevier, 2019, pp. 815–843.

[84] L. Yang, A. Hakki, L. Zheng, M.R. Jones, F. Wang, D.E. Macphee, Photocatalytic concrete for NO_x abatement: supported TiO₂ efficiencies and impacts, *Cem. Concr. Res.* 116 (2019) 57–64.

[85] M.A. Mohd Adnan, N. Muhd Jukapli, M.N.I. Amir, A. Maamor, Effect on different TiO₂ photocatalyst supports on photodecolorization of synthetic dyes: a review, *Int. J. Environ. Sci. Technol.* 16 (2019) 547–566.

[86] W. Zou, B. Gao, Y.S. Ok, L. Dong, Integrated adsorption and photocatalytic degradation of volatile organic compounds (VOCs) using carbon-based nanocomposites: a critical review, *Chemosphere* 218 (2019) 845–859.

[87] C. Liu, R. Zhang, S. Wei, J. Wang, Y. Liu, M. Li, R. Liu, Selective removal of H₂S from biogas using a regenerable hybrid TiO₂/zeolite composite, *Fuel* 157 (2015) 183–190.

[88] X. Yu, J. Hao, Z. Xi, T. Liu, Y. Lin, B. Xu, Investigation of low concentration SO₂ adsorption performance on different amine-modified Merrifield resins, *Atmos. Pollut. Res.* 10 (2019) 404–411.

[89] R. Kapoor, P. Ghosh, M. Kumar, V.K. Vijay, Evaluation of biogas upgrading technologies and future perspectives: a review, *Environ. Sci. Pollut. Res.* (2019).

[90] F.M. Baena-Moreno, M. Rodríguez-Galán, F. Vega, L.F. Vilches, B. Navarrete, Z. Zhang, Biogas upgrading by cryogenic techniques, *Environ. Chem. Lett.* (2019).

[91] D. Puparelo, S. Silvestri, A. Lanzini, Biogas cleaning: trace compounds removal with model validation, *Sep. Purif. Technol.* 210 (2019) 80–92.

[92] R. Portela, S. Suárez, S.B. Rasmussen, N. Arconada, Y. Castro, A. Durán, P. Ávila, J.M. Coronado, B. Sánchez, Photocatalytic-based strategies for H₂S elimination, *Catal. Today* 151 (2010) 64–70.

[93] S.B. Rasmussen, R. Portela, S. Suárez, J.M. Coronado, M.-L. Rojas-Cervantes, P. Avila, B. Sánchez, Hybrid TiO₂–SiMgOX composite for combined chemisorption and photocatalytic elimination of gaseous H₂S, *Ind. Eng. Chem. Res.* 49 (2010) 6685–6690.

[94] Q. Wu, H. Yang, H. Zhu, Z. Gao, Construction of CNCs-TiO₂ heterojunctions with enhanced photocatalytic activity for crystal violet removal, *Optik* 179 (2019) 195–206.

[95] J. Yan, G. Wu, N. Guan, L. Li, Nb₂O₅/TiO₂ heterojunctions: synthesis strategy and photocatalytic activity, *Appl. Catal. B Environ.* 152–153 (2014) 280–288.

[96] M.A. Behnajady, B. Alizade, Enhancement of TiO₂-UV100 nanoparticles photocatalytic activity by Mg impregnation in the removal of a model organic pollutant, *Desalin. Water Treat.* 53 (2015) 689–696.

[97] M. Covei, D. Perniu, C. Bogatu, A. Dutu, CZTS-TiO₂ thin film heterostructures for advanced photocatalytic wastewater treatment, *Catal. Today* 321–322 (2019) 172–177.

[98] Y. Poo-arporn, S. Kityakarn, A. Niltharach, M.F. Smith, S. Seraphin, M. Wörner,

A. Worayingpong, Photocatalytic oxidation of thiophene over cerium doped TiO₂ thin film, *Mater. Sci. Semicond. Process.* 93 (2019) 21–27.

[99] A.E. Kabeel, R. Sathyamurthy, S.W. Sharshir, A. Muthumanokar, H. Panchal, N. Prakash, C. Prasad, S. Nandakumar, M.S. El Kady, Effect of water depth on a novel absorber plate of pyramid solar still coated with TiO₂ nano black paint, *J. Clean. Prod.* 213 (2019) 185–191.

[100] A.T. Saber, A. Mortensen, J. Szarek, N.R. Jacobsen, M. Levin, I.K. Koponen, K.A. Jensen, U. Vogel, H. Wallin, Toxicity of pristine and paint-embedded TiO₂ nanomaterials, *Hum. Exp. Toxicol.* 38 (2018) 11–24.

[101] T. Martinez, A. Bertron, E. Ringot, G. Escadeillas, Degradation of NO using photocatalytic coatings applied to different substrates, *Build. Environ.* 46 (2011) 1808–1816.

[102] E.B. Lied, C.F.M. Morejon, R.L.O. Basso, A.P. Trevisan, P.R.S. Bittencourt, F.L. Fronza, Photocatalytic degradation of H₂S in the gas-phase using a continuous flow reactor coated with TiO₂-based acrylic paint, *Environ. Technol.* (2018) 1–14.

[103] M. Brancher, D. Franco, H. de Melo Lisboa, Photocatalytic oxidation of H₂S in the gas phase over TiO₂-coated glass fiber filter, *Environ. Technol.* 37 (2016) 2852–2864.

[104] L.-Y. Xia, D.-H. Gu, J. Tan, W.-B. Dong, H.-Q. Hou, Photolysis of low concentration H₂S under UV/VUV irradiation emitted from microwave discharge electrodeless lamps, *Chemosphere* 71 (2008) 1774–1780.

[105] J. Xu, C. Li, P. Liu, D. He, J. Wang, Q. Zhang, Photolysis of low concentration H₂S under UV/VUV irradiation emitted from high frequency discharge electrodeless lamps, *Chemosphere* 109 (2014) 202–207.

[106] M. Wu, D.Y.C. Leung, Y. Zhang, H. Huang, R. Xie, W. Szeto, F. Li, Toluene degradation over Mn-TiO₂/CeO₂ composite catalyst under vacuum ultraviolet (VUV) irradiation, *Chem. Eng. Sci.* 195 (2019) 985–994.

[107] H. Huang, G. Liu, Y. Zhan, Y. Xu, H. Lu, H. Huang, Q. Feng, M. Wu, Photocatalytic oxidation of gaseous benzene under VUV irradiation over TiO₂/Zeolites catalysts, *Catal. Today* 281 (2017) 649–655.

[108] S. Mohan, P. Saranya, A novel bagging ensemble approach for predicting summertime ground-level ozone concentration, *J. Air Waste Manage. Assoc.* 69 (2019) 220–233.

[109] M. Wu, Y. Zhang, W. Szeto, W. Pan, H. Huang, D.Y.C. Leung, Vacuum ultraviolet (VUV)-based photocatalytic oxidation for toluene degradation over pure CeO₂, *Chem. Eng. Sci.* 200 (2019) 203–213.

[110] Y. Shu, M. He, J. Ji, H. Huang, S. Liu, D.Y.C. Leung, Synergetic degradation of VOCs by vacuum ultraviolet photolysis and catalytic ozonation over Mn-xCe/ZSM-5, *J. Hazard. Mater.* 364 (2019) 770–779.

[111] Y. Wang, Z. Wang, J. Pan, Y. Liu, Removal of gaseous hydrogen sulfide using Fenton reagent in a spraying reactor, *Fuel* 239 (2019) 70–75.

[112] G. Liu, J. Ji, P. Hu, S. Lin, H. Huang, Efficient degradation of H₂S over transition metal modified TiO₂ under VUV irradiation: performance and mechanism, *Appl. Surf. Sci.* 433 (2018) 329–335.

[113] A.J. Moreira, A.C. Borges, B.B. de Souza, L.R. Barbosa, V.R. de Mendonça, C.D. Freschi, G.P.G. Freschi, Microwave discharge electrodeless mercury lamp (Hg-MDEL): an energetic, mechanistic and kinetic approach to the degradation of Prozac®, *J. Environ. Chem. Eng.* 7 (2019) 102916.

[114] L. Youssef, G. Younes, R. Al-Oweini, Photocatalytic degradation of atrazine by heteropolyoxotungstates, *J. Taibah Univ. Sci.* 13 (2019) 274–279.

[115] Y. Yu, T. Zhang, L. Zheng, J. Yu, Photocatalytic degradation of hydrogen sulfide using TiO₂ film under microwave electrodeless discharge lamp irradiation, *Chem. Eng. J.* 225 (2013) 9–15.

[116] J.L. Coutts, L.H. Levine, J.T. Richards, D.W. Mazyck, The effect of photon source on heterogeneous photocatalytic oxidation of ethanol by a silica-titania composite, *J. Photochem. Photobiol. A: Chem.* 225 (2011) 58–64.

[117] G. Vincent, P.M. Marquaire, O. Zahraa, Abatement of volatile organic compounds using an annular photocatalytic reactor: study of gaseous acetone, *J. Photochem. Photobiol. A: Chem.* 197 (2008) 177–189.

[118] J.-M. Herrmann, Heterogeneous photocatalysis: fundamentals and applications to the removal of various types of aqueous pollutants, *Catal. Today* 53 (1999) 115–129.

[119] J.-M. Herrmann, Fundamentals and misconceptions in photocatalysis, *J. Photochem. Photobiol. A: Chem.* 216 (2010) 85–93.

[120] F. Zhou, C. Yan, Q. Sun, S. Komarneni, TiO₂/Sepiolite nanocomposites doped with rare earth ions: preparation, characterization and visible light photocatalytic activity, *Microporous Mesoporous Mater.* 274 (2019) 25–32.

[121] B. Deng, C. Xu, Z. Li, W. Huang, Q. Wu, Y. Zhang, M. Ni, K. Cen, Enhanced solar conversion of CO₂ to CO using Mn-doped TiO₂ based on photo-thermochemical cycle, *ChemistrySelect* 4 (2019) 236–244.

[122] S.Y. Mendiola-Alvarez, J.L. Guzmán-Mar, G. Turnes-Palomino, F. Maya-Alejandro, A. Caballero-Quintero, A. Hernández-Ramírez, L. Hinjozosa-Reyes, Synthesis of Cr₃₊-doped TiO₂ nanoparticles: characterization and evaluation of their visible photocatalytic performance and stability, *Environ. Technol.* 40 (2019) 144–153.

[123] Z. Wang, X. Ci, H. Dai, L. Yin, H. Shi, One-step synthesis of highly active Ti-containing Cr-modified MCM-48 mesoporous material and the photocatalytic performance for decomposition of H₂S under visible light, *Appl. Surf. Sci.* 258 (2012) 8258–8263.

[124] L. Davydov, E.P. Reddy, P. France, P.G. Smirniotis, Transition-metal-Substituted titania-loaded MCM-41 as photocatalysts for the degradation of aqueous organics in visible light, *J. Catal.* 203 (2001) 157–167.

[125] M. Anpo, T.-H. Kim, M. Matsuoka, The design of Ti-, V-, Cr-oxide single-site catalysts within zeolite frameworks and their photocatalytic reactivity for the decomposition of undesirable molecules—the role of their excited states and reaction mechanisms, *Catal. Today* 142 (2009) 114–124.

[126] S. Wei, F. Wang, M. Dan, K. Zeng, Y. Zhou, The role of high oxygen vacancy concentration on modification of surface properties and H₂S adsorption on the rutile TiO₂ (110), *Appl. Surf. Sci.* 422 (2017) 990–996.

[127] F. Zuo, L. Wang, T. Wu, Z. Zhang, D. Borchardt, P. Feng, Self-doped Ti₃₊ enhanced photocatalyst for hydrogen production under visible light, *J. Am. Chem. Soc.* 132 (2010) 11856–11857.

[128] D.C. Cronemeyer, Infrared absorption of reduced rutile TiO₂ single crystals, *Phys. Rev.* 113 (1959) 1222–1226.

[129] G. Lu, A. Linsebigler, J.T. Yates, The adsorption and photodesorption of oxygen on the TiO₂(110) surface, *J. Chem. Phys.* 102 (1995) 4657–4662.

[130] F. Wang, S. Wei, Z. Zhang, G.R. Patzke, Y. Zhou, Oxygen vacancies as active sites for H₂S dissociation on the rutile TiO₂(110) surface: a first-principles study, *Phys. Chem. Chem. Phys.* 18 (2016) 6706–6712.

[131] X. Li, G. Zhang, H. Pan, Experimental study on ozone photolytic and photocatalytic degradation of H₂S using continuous flow mode, *J. Hazard. Mater.* 199–200 (2012) 255–261.

[132] A.M. Abdel-Mageed, S. Eckle, H.G. Anfang, R.J. Behm, Selective CO methanation in CO₂-rich H₂ atmospheres over a Ru/zeolite catalyst: the influence of catalyst calcination, *J. Catal.* 298 (2013) 148–160.

[133] Y. Kuwahara, J. Aoyama, K. Miyakubo, T. Eguchi, T. Kamegawa, K. Mori, H. Yamashita, TiO₂ photocatalyst for degradation of organic compounds in water and air supported on highly hydrophobic FAU zeolite: structural, sorptive, and photocatalytic studies, *J. Catal.* 285 (2012) 223–234.

[134] A. Alonso-Tellez, D. Robert, N. Keller, V. Keller, A parametric study of the UV-A photocatalytic oxidation of H₂S over TiO₂, *Appl. Catal. B Environ.* 115–116 (2012) 209–218.

[135] E. Sánchez-González, P.G.M. Mileo, M. Sagastuy-Breña, J.R. Álvarez, J.E. Reynolds, A. Villarreal, A. Gutiérrez-Alejandro, J. Ramírez, J. Balmaseda, E. González-Zamora, G. Maurin, S.M. Humphrey, I.A. Ibarra, Highly reversible sorption of H₂S and CO₂ by an environmentally friendly Mg-based MOF, *J. Mater. Chem. A* 6 (2018) 16900–16909.

[136] F. Yazdanbakhsh, J.A. Sawada, M. Alizadehgiashi, M. Mohammadmalipour, S.M. Kuznicki, Effect of moisture on high temperature H₂S adsorption by copper-exchanged Engelhard Titanosilicate-2, *J. Nanosci. Nanotechnol.* 17 (2017) 3409–3414.

[137] A.J. Jafari, R.R. Kalantari, M. Kermani, M.H. Firooz, Photocatalytic oxidation of benzene by ZnO coated on glass plates under simulated sunlight, *Chem. Pap.* 73 (2019) 635–644.

[138] M. Grzeskowiak, R.J. Wróbel, D. Moszyński, S. Mozia, J. Grzechulska-Damszel, A.W. Morawski, J. Przepiórski, TiO₂ supported on quartz wool for photocatalytic oxidation of hydrogen sulphide, *Adsorpt. Sci. Technol.* 32 (2014) 765–773.

[139] L. Cheng, Q. Xiang, Y. Liao, H. Zhang, Cds-Based photocatalysts, *Energy Environ. Sci.* 11 (2018) 1362–1391.

[140] P. Sánchez-Cid, C. Jaramillo-Páez, J.A. Navío, A.N. Martín-Gómez, M.C. Hidalgo, Coupling of Ag₂CO₃ to an optimized ZnO photocatalyst: advantages vs. Disadvantages, *J. Photochem. Photobiol. A: Chem.* 369 (2019) 119–132.

[141] S. Fu, Y. Zheng, X. Zhou, Z. Ni, S. Xia, Visible light promoted degradation of gaseous volatile organic compounds catalyzed by Au supported layered double hydroxides: influencing factors, kinetics and mechanism, *J. Hazard. Mater.* 363 (2019) 41–54.

[142] B. Lu, X. Wang, L. Li, Y. Du, W. Chen, Y. Liu, Direct spectroscopic evidence on the photocatalytic activities of different ZnO crystal facets toward photo-induced decomposition of CH₂O, *Appl. Surf. Sci.* 478 (2019) 62–67.

[143] P. Zhang, S. Wang, B.Y. Guan, X.W. Lou, Fabrication of CdS hierarchical multi-cavity hollow particles for efficient visible light CO₂ reduction, *Energy Environ. Sci.* 12 (2019) 164–168.

[144] V. Preethi, S. Kammani, Optimization of operating parameters for gas-phase photocatalytic splitting of H₂S by novel vermiculite packed tubular reactor, *J. Environ. Manage.* 181 (2016) 674–680.

[145] D. Huang, S. Chen, G. Zeng, X. Gong, C. Zhou, M. Cheng, W. Xue, X. Yan, J. Li, Artificial Z-scheme photocatalytic system: What have been done and where to go? *Coord. Chem. Rev.* 385 (2019) 44–80.

[146] H. Li, H. Hu, C. Bao, F. Guo, X. Zhang, X. Liu, J. Hua, J. Tan, A. Wang, H. Zhou, B. Yang, Y. Qu, X. Liu, Forming heterojunction: an effective strategy to enhance the photocatalytic efficiency of a new metal-free organic photocatalyst for water splitting, *Sci. Rep.* 6 (2016) 29327.

[147] J. Low, J. Yu, M. Jaroniec, S. Wageh, A.A. Al-Ghamdi, Heterojunction photocatalysts, *Adv. Mater.* 29 (2017) 1601694.

[148] H. Hitha, A. Jose, T. Varghese, Synthesis, characterization and photocatalytic activity of NiWO₄ nanoparticles, *AIP Conference Proceedings* 2082 (2019) 030017.

[149] M. Kang, X. Wang, J. Zhang, Y. Lu, X. Chen, L. Yang, F. Wang, Boosting the photocatalytic oxidative desulfurization of dibenzothiophene by decoration of MWo4 (M=Ca, Zn, Ni) on WO₃, *J. Environ. Chem. Eng.* 7 (2019) 102809.

[150] J. Ke, M. Adnan Younis, Y. Kong, H. Zhou, J. Liu, L. Lei, Y. Hou, Nanostructured ternary metal tungstate-based photocatalysts for environmental purification and solar water splitting: a review, *Nano-Micro Lett.* 10 (2018) 69.

[151] D. Xing, Y. Liu, P. Zhou, Z. Wang, P. Wang, Z. Zheng, X. Zhang, X. Qin, Y. Dai, B. Huang, Enhanced photocatalytic hydrogen evolution of CdWO₄ through polar organic molecule modification, *Int. J. Hydrogen Energy* 44 (2019) 4754–4763.

[152] Y.A. Sethi, R.P. Panmand, S.R. Kadam, A.K. Kulkarni, S.K. Apte, S.D. Naik, N. Munirathnam, M.V. Kulkarni, B.B. Kale, Nanostructured CdS sensitized CdWO₄ nanorods for hydrogen generation from hydrogen sulfide and dye degradation under sunlight, *J. Colloid Interface Sci.* 487 (2017) 504–512.

[153] N.A. Zakaria, L.D. Volkova, O.K. Kim, A.R. Brodskii, I.F. Latypov, V.I. Yaskevich, L.V. Komashko, Natural iron-containing materials and catalysts on their basis on use for photocatalytic decomposition of hydrogen sulfide, *Pet. Chem.* 53 (2013) 17

181–186.

[154] P. Dias, A. Mendes, Hydrogen production from photoelectrochemical Water splitting, in: T.E. Lipman, A.Z. Weber (Eds.), *Fuel Cells and Hydrogen Production: A Volume in the Encyclopedia of Sustainability Science and Technology*, second edition, Springer, New York, New York, NY, 2019, pp. 1003–1053.

[155] Y. Zhang, S. Kumar, F. Marken, M. Krasny, E. Roake, S. Eslava, S. Dunn, E. Da Como, C.R. Bowen, Pyro-electrolytic water splitting for hydrogen generation, *Nano Energy* 58 (2019) 183–191.

[156] M. Dan, S. Wei, D.E. Doronkin, Y. Li, Z. Zhao, S. Yu, J.-D. Grunwaldt, Y. Lin, Y. Zhou, Novel MnS/(InxCu1-x)2S3 composite for robust solar hydrogen sulphide splitting via the synergy of solid solution and heterojunction, *Appl. Catal. B Environ.* 243 (2019) 790–800.

[157] A. Fujishima, K. Honda, Electrochemical photolysis of water at a semiconductor electrode, *Nature* 238 (1972) 37–38.

[158] M. Dan, Q. Zhang, S. Yu, A. Prakash, Y. Lin, Y. Zhou, Noble-metal-free MnS/In2S3 composite as highly efficient visible light driven photocatalyst for H2 production from H2S, *Appl. Catal. B Environ.* 217 (2017) 530–539.

[159] Z. Li, Q. Zhang, M. Dan, Z. Guo, Y. Zhou, A facile preparation route of Bi2S3 nanorod films for photocatalytic H2 production from H2S, *Mater. Lett.* 201 (2017) 118–121.

[160] A. Prakash, M. Dan, S. Yu, S. Wei, Y. Li, F. Wang, Y. Zhou, In2S3/CuS nanosheet composite: an excellent visible light photocatalyst for H2 production from H2S, *Sol. Energy Mater. Sol. Cells* 180 (2018) 205–212.

[161] Z. Li, Z. Zhou, J. Ma, Y. Li, W. Peng, G. Zhang, F. Zhang, X. Fan, Hierarchical photocatalyst of In2S3 on exfoliated MoS2 nanosheets for enhanced visible-light-driven Aza-Henry reaction, *Appl. Catal. B Environ.* 237 (2018) 288–294.

[162] Y. Zhong, G. Zhao, F. Ma, Y. Wu, X. Hao, Utilizing photocorrosion-recrystallization to prepare a highly stable and efficient CdS/WS2 nanocomposite photocatalyst for hydrogen evolution, *Appl. Catal. B Environ.* 199 (2016) 466–472.

[163] G. Ma, H. Yan, J. Shi, X. Zong, Z. Lei, C. Li, Direct splitting of H2S into H2 and S on CdS-based photocatalyst under visible light irradiation, *J. Catal.* 260 (2008) 134–140.

[164] M. Dan, J. Xiang, F. Wu, S. Yu, Q. Cai, L. Ye, Y. Ye, Y. Zhou, Rich active-edge-site MoS2 anchored on reduction sites in metal sulfide heterostructure: toward robust visible light photocatalytic hydrogen sulphide splitting, *Appl. Catal. B Environ.* 256 (2019) 117870.

[165] X. She, H. Xu, L. Li, Z. Mo, X. Zhu, Y. Yu, Y. Song, J. Wu, J. Qian, S. Yuan, H. Li, Steering charge transfer for boosting photocatalytic H2 evolution: integration of two-dimensional semiconductor superiorities and noble-metal-free Schottky junction effect, *Appl. Catal. B Environ.* 245 (2019) 477–485.

[166] B. Wang, S. He, L. Zhang, X. Huang, F. Gao, W. Feng, P. Liu, CdS nanorods decorated with inexpensive NiCd bimetallic nanoparticles as efficient photocatalysts for visible-light-driven photocatalytic hydrogen evolution, *Appl. Catal. B Environ.* 243 (2019) 229–235.

[167] J. Low, B. Dai, T. Tong, C. Jiang, J. Yu, In situ irradiated X-Ray photoelectron spectroscopy investigation on a direct Z-Scheme TiO2/CdS composite film photocatalyst, *Adv. Mater.* 31 (2019) 1802981.

[168] Y. Li, S. Yu, D.E. Doronkin, S. Wei, M. Dan, F. Wu, L. Ye, J.-D. Grunwaldt, Y. Zhou, Highly dispersed PdS preferably anchored on In2S3 of MnS/In2S3 composite for effective and stable hydrogen production from H2S, *J. Catal.* 373 (2019) 48–57.

[169] J.S. Jang, H. Gyu Kim, P.H. Borse, J.S. Lee, Simultaneous hydrogen production and decomposition of H2S dissolved in alkaline water over CdS-TiO2 composite photocatalysts under visible light irradiation, *Int. J. Hydrogen Energy* 32 (2007) 4786–4791.

[170] M. Patil, D. Sharma, A. Dive, S. Mahajan, R. Sharma, Synthesis and characterization of Cu2S thin film deposited by chemical bath deposition method, *Procedia Manuf.* 20 (2018) 505–508.

[171] Y. Tang, D. Zhang, X. Pu, B. Ge, Y. Li, Y. Huang, Snowflake-like Cu2S/Zn0.5Cd0.5S p-n heterojunction photocatalyst for enhanced visible light photocatalytic H2 evolution activity, *J. Taiwan Inst. Chem. Eng.* 96 (2019) 487–495.

[172] R.J. Vimal Michael, J. Theerthagiri, J. Madhavan, M.J. Umaphathy, P.T. Manoharan, Cu2S-incorporated ZnS nanocomposites for photocatalytic hydrogen evolution, *RSC Adv.* 5 (2015) 30175–30186.

[173] H. Huang, F. Li, H. Wang, X. Zheng, The size controlled synthesis of Cu2S/P25 hetero junction solar-energy-materials and their applications in photocatalytic degradation of dyes, *RSC Adv.* 7 (2017) 50056–50063.

[174] V. Navakoteswara Rao, N. Lakshmana Reddy, M. Mamatha Kumari, P. Ravi, M. Sathish, K.M. Kuruvila, V. Preethi, K.R. Reddy, N.P. Shetti, T.M. Aminabhavi, M.V. Shankar, Photocatalytic recovery of H2 from H2S containing wastewater: surface and interface control of photo-excitons in Cu2S@TiO2 core-shell nanostructures, *Appl. Catal. B Environ.* 254 (2019) 174–185.

[175] N.L. Reddy, S. Kumar, V. Krishnan, M. Sathish, M.V. Shankar, Multifunctional Cu/Ag quantum dots on TiO2 nanotubes as highly efficient photocatalysts for enhanced solar hydrogen evolution, *J. Catal.* 350 (2017) 226–239.

[176] J. Yu, L. Qi, M. Jaroniec, Hydrogen production by photocatalytic water splitting over Pt/TiO2 nanosheets with exposed (001) facets, *J. Phys. Chem. C* 114 (2010) 13118–13125.

[177] K. Mondal, A. Sharma, Recent advances in the synthesis and application of photocatalytic metal–metal oxide core–shell nanoparticles for environmental remediation and their recycling process, *RSC Adv.* 6 (2016) 83589–83612.

[178] N. Sakamoto, H. Ohtsuka, T. Ikeda, K. Maeda, D. Lu, M. Kanehara, K. Teramura, T. Teranishi, K. Domen, Highly dispersed noble-metal/chromia (core/shell) nanoparticles as efficient hydrogen evolution promoters for photocatalytic overall water splitting under visible light, *Nanoscale* 1 (2009) 106–109.

[179] H. Sun, Z. Jiang, D. Wu, L. Ye, T. Wang, B. Wang, T. An, P.K. Wong, Defect-type-Dependent near-infrared-driven photocatalytic bacterial inactivation by defective Bi2S3 nanorods, *ChemSusChem* 12 (2019) 890–897.

[180] X. Xu, L. Meng, Y. Li, C. Sun, S. Yang, H. He, Bi2S3 nanoribbons-hybridized {001} facets exposed Bi2WO6 ultrathin nanosheets with enhanced visible light photocatalytic activity, *Appl. Surf. Sci.* 479 (2019) 410–422.

[181] J. Kaur, M. Sharma, O.P. Pandey, Photoluminescence and photocatalytic studies of metal ions (Mn and Ni) doped ZnS nanoparticles, *Opt. Mater.* 47 (2015) 7–17.

[182] R. Wang, H. Liang, J. Hong, Z. Wang, Hydrothermal synthesis of cobalt-doped ZnS for efficient photodegradation of methylene blue, *J. Photochem. Photobiol. A: Chem.* 325 (2016) 62–67.

[183] A. Kay, I. Cesar, M. Grätzel, New benchmark for water photooxidation by nanostructured α -Fe2O3 films, *J. Am. Chem. Soc.* 128 (2006) 15714–15721.

[184] M. Lashgari, M. Ghanimati, Photocatalytic degradation of H2S aqueous media using sulfide nanostructured solid-solution solar-energy-materials to produce hydrogen fuel, *J. Hazard. Mater.* 345 (2018) 10–17.

[185] M. Lashgari, P. Elyas-Haghghi, M. Takeguchi, A highly efficient p-n junction nanocomposite solar-energy-material [nano-photovoltaic] for direct conversion of water molecules to hydrogen solar fuel, *Sol. Energy Mater. Sol. Cells* 165 (2017) 9–16.

[186] Z. Ambrus, N. Baláz, T. Alapi, G. Wittmann, P. Sipos, A. Dombi, K. Mogyorósi, Synthesis, structure and photocatalytic properties of Fe(III)-doped TiO2 prepared from TiCl3, *Appl. Catal. B Environ.* 81 (2008) 27–37.

[187] D. Dvoranová, V. Brezová, M. Mazúr, M.A. Malati, Investigations of metal-doped titanium dioxide photocatalysts, *Appl. Catal. B Environ.* 37 (2002) 91–105.

[188] S.A. Ansari, M.M. Khan, M.O. Ansari, M.H. Cho, Nitrogen-doped titanium dioxide (N-doped TiO2) for visible light photocatalysis, *New J. Chem.* 40 (2016) 3000–3009.

[189] A.P. Bhirud, S.D. Sathaye, R.P. Waichal, J.D. Ambekar, C.-J. Park, B.B. Kale, In-situ preparation of N-TiO2/graphene nanocomposite and its enhanced photocatalytic hydrogen production by H2S splitting under solar light, *Nanoscale* 7 (2015) 5023–5034.

[190] M. Ahmed, A. Giwa, S.W. Hasan, Chapter 26 - Challenges and opportunities of graphene-based materials in current desalination and water purification technologies, in: S. Thomas, D. Pasquini, S.-Y. Leu, D.A. Gopakumar (Eds.), *Nanoscale Materials in Water Purification*, Elsevier, 2019, pp. 735–758.

[191] M. Safarpour, A. Khataee, Chapter 15 - Graphene-based materials for water purification, in: S. Thomas, D. Pasquini, S.-Y. Leu, D.A. Gopakumar (Eds.), *Nanoscale Materials in Water Purification*, Elsevier, 2019, pp. 383–430.

[192] H. Wang, Q. Liu, C. You, Regeneration of sulfur-deactivated TiO2 photocatalysts, *Appl. Catal. A Gen.* 572 (2019) 15–23.

[193] H. Sheng, D. Chen, N. Li, Q. Xu, H. Li, J. He, J. Lu, Urchin-inspired TiO2@MIL-101 double-shell hollow particles: adsorption and highly efficient photocatalytic degradation of hydrogen sulfide, *Chem. Mater.* 29 (2017) 5612–5616.

[194] G. Zhang, H. Sheng, D. Chen, N. Li, Q. Xu, H. Li, J. He, J. Lu, Hierarchical titanium dioxide Nanowire/Metal–Organic Framework/Carbon nanofiber membranes for highly efficient photocatalytic degradation of hydrogen sulfide, *Chem. Eur. J.* 24 (2018) 15019–15025.

[195] S. Kataoka, E. Lee, M.I. Tejedor-Tejedor, M.A. Anderson, Photocatalytic degradation of hydrogen sulfide and in situ FT-IR analysis of reaction products on surface of TiO2, *Appl. Catal. B Environ.* 61 (2005) 159–163.

[196] N. Serpone, Relative photonic efficiencies and quantum yields in heterogeneous photocatalysis, *J. Photochem. Photobiol. A: Chem.* 104 (1997) 1–12.

[197] N. Serpone, R. Terzian, D. Lawless, P. Kennepohl, G. Sauvé, On the usage of turnover numbers and quantum yields in heterogeneous photocatalysis, *J. Photochem. Photobiol. A: Chem.* 73 (1993) 11–16.

[198] H. Kisch, D. Bahnenmann, Best practice in photocatalysis: comparing rates or apparent quantum yields? *J. Phys. Chem. Lett.* 6 (2015) 1907–1910.

[199] G.J. Janz, S.C. Wait, Space-time yield and reaction rate, *J. Chem. Phys.* 23 (1955) 1550–1551.

[200] J. Ji, Y. Xu, H. Huang, M. He, S. Liu, G. Liu, R. Xie, Q. Feng, Y. Shu, Y. Zhan, R. Fang, X. Ye, D.Y.C. Leung, Mesoporous TiO2 under VUV irradiation: enhanced photocatalytic oxidation for VOCs degradation at room temperature, *Chem. Eng. J.* 327 (2017) 490–499.

[201] S. Rezaei, A.M. Avila, S.M. Kuznicki, Chemisorption of H2S on Copper-ETS-2: experiment and modeling of a packed column, *J. Nanosci. Nanotechnol.* 18 (2018) 7882–7888.

[202] F. Shen, J. Liu, Z. Zhang, Y. Dong, C. Gu, Density functional study of hydrogen sulfide adsorption mechanism on activated carbon, *Fuel Process. Technol.* 171 (2018) 258–264.

[203] K. Vikrant, C.M. Park, K.-H. Kim, S. Kumar, E.-C. Jeon, Recent Advancements in Photocatalyst-based Platforms for the Destruction of Gaseous Benzene: Performance Evaluation of Different Modes of Photocatalytic Operations and Against Adsorption Techniques, Unpublished work (Submitted) (2019).

[204] N. Yaghobi, The role of gas hourly space velocity and feed composition for catalytic oxidative coupling of methane: experimental study, *J. King Saud Univ. - Eng. Sci.* 25 (2013) 1–10.

[205] A. Khan, J.E. Szulejko, K.-H. Kim, P. Sammadar, S.S. Lee, X. Yang, Y.S. Ok, A comparison of figure of merit (FOM) for various materials in adsorptive removal of benzene under ambient temperature and pressure, *Environ. Res.* 168 (2019) 96–108.

[206] N. Bindra, M. Karim, Balancing between two extremes during environmental impact assessment: a case study, *Environ. Process.* 6 (2019) 283–307.

[207] A.M. Khan, V.M. Rao, Q. Li, Recent advances in electrochemical sensors for detecting toxic gases: NO2, SO2 and H2S, *Sensors* 19 (2019).

[208] L. Tang, Y. Lin, X. He, G. Han, Acid rain decelerates the decomposition of Cunninghamia lanceolata needle and Cinnamomum camphora leaf litters in a karst region in China, *Ecol. Res.* 34 (2019) 193–200.

[209] Y. Yang, J. Liu, F. Liu, Z. Wang, Z. Zhang, Comprehensive evolution mechanism of SO_x formation during pyrite oxidation, *Proc. Combust. Inst.* 37 (2019) 2809–2819.

[210] X. Pi, F. Sun, J. Gao, Z. Qu, A. Wang, Z. Qie, L. Wang, H. Liu, A new insight into the SO₂ adsorption behavior of oxidized carbon materials using model adsorbents and DFT calculations, *Phys. Chem. Chem. Phys.* (2019).

[211] K. Silas, W.A.W.A.K. Ghani, T.S.Y. Choong, U. Rashid, Carbonaceous materials modified catalysts for simultaneous SO₂/NO_x removal from flue gas: a review, *Catal. Rev.* 61 (2019) 134–161.

[212] K. Yang, H. Yi, X. Tang, S. Zhao, F. Gao, Y. Huang, Z. Yang, J. Wang, Y. Shi, X. Xie, Reducing the competitive adsorption between SO₂ and NO by Al₂O₃@TiO₂ core-shell structure adsorbent, *Chem. Eng. J.* 364 (2019) 420–427.

[213] E.L. Cates, Photocatalytic water treatment: so where are we going with this? *Environ. Sci. Technol.* 51 (2017) 757–758.

[214] X. Hao, G. Hou, P. Zheng, R. Liu, C. Liu, H₂S in-situ removal from biogas using a tubular zeolite/TiO₂ photocatalytic reactor and the improvement on methane production, *Chem. Eng. J.* 294 (2016) 105–110.

[215] M.-H. Lee, K. Vikrant, S.A. Younis, J.E. Szulejko, K.-H. Kim, The Most Powerful Platform for the Removal of Hydrogen Sulfide: MOF-199 Over Other Frameworks and Commercial Sorbents and Insights Into Its Capture Mechanisms, Unpublished work (Submitted) (2019).

[216] Sigma-Aldrich, Sigma-Aldrich Chemical Catalog, (2019) <https://www.sigmaaldrich.com/korea.html>.